https://doi.org/10.5194/egusphere-2025-1602
Preprint. Discussion started: 8 May 2025

Optimizing CCN predictions through inferred modal aerosol composition – a boreal forest case study

Rahul Ranjan[1, 2], Liine Heikkinen [1, 2], Lauri R. Ahonen[3], Krista Luoma[3, 6], Paul Bowen[5], Tuukka Petäjä[3], Annica M. L. Ekman[4, 2], Daniel G. Partridge[5] and Ilona Riipinen[1, 2]

[1]Department of Environmental Science (ACES), Stockholm University, 10691, Stockholm, Sweden
[2]Bolin Centre for Climate Research, Stockholm University, 10691, Stockholm, Sweden
[3]Institute for Atmospheric and Earth System Research/Physics, University of Helsinki, 00014, Helsinki, Finland
[4]Department of Meteorology, Stockholm University, Stockholm, Sweden
[5]Department of Mathematics and Statistics, Faculty of Environment, Science and Economy, University of Exeter, EX4 4QF, Exeter, United Kingdom
[6]Atmospheric Composition Research, Finnish Meteorological Institute, Helsinki, 00560, Finland

Correspondence to: Rahul Ranjan (rahul.ranjan@aces.su.se) and Ilona Riipinen (ilona.riipinen@aces.su.se)

Abstract

The contribution of natural aerosol particles from boreal forests to total aerosol loadings may increases with anticipated reduction in anthropogenic emissions. It is therefore pertinent to understand the cloud-forming potential of these particles. Observational data on aerosol particle number size distribution and chemical composition is required for predicting cloud condensation nuclei (CCN) concentrations. However, long-term online measurements of chemical composition typically provide data on total sub-micron particulate mass, which only represents the larger end of the number size distribution. To bridge this gap, we employed κ-Köhler theory on a multi-year (2016–2020) dataset from Hyytiälä, southern Finland, to investigate improved closure between observed and predicted CCN concentrations by optimizing the size-resolved chemical composition. This optimization improved the CCN closure primarily at supersaturations above 0.5 % where the Aitken mode makes a substantial contribution to the CCN number. The optimization suggested inorganic enrichment in the accumulation mode compared to organic enrichment in the Aitken mode. The mass fractions of inorganics in the two modes vary with season, the greatest difference taking place in winter (+156% in the accumulation mode as compared with Aitken mode) and smallest in summer (+52%). These results reflect the contributions from long-range transport and chemical cloud processing as well as the pivotal role of organic vapors in facilitating the growth of newly-formed particles towards CCN-sizes. Our study demonstrates the potential for utilizing CCN measurements for inferring information on the parts of the aerosol size distribution that are beyond the reach of traditional online composition measurements.

https://doi.org/10.5194/egusphere-2025-1602
Preprint. Discussion started: 8 May 2025

1 Introduction

Aerosol particles are important in the formation of cloud droplets as they serve as cloud condensation nuclei (CCN) by lowering the energy barrier for heterogeneous nucleation of water and hence cloud droplet activation in atmospheric levels of water vapor supersaturations *SS* (Köhler 1921; Pruppacher and Klett, 2010). The subset of aerosol particles that act as CCN, in turn, affects the cloud droplet number concentration (CDNC), thereby changes in the CCN concentration (N_{CCN}) may modulate cloud radiative properties and lifetime — phenomena known as the first (Twomey, 1974) and second (Albrecht, 1989) indirect aerosol climate effects. The parameterization schemes related to cloud droplet formation in global climate models (e.g., Abdul-Razzak and Ghan, 2000, 2002; Nenes and Seinfeld, 2003; Fountoukis and Nenes, 2005; Barahona et al., 2010; Betancourt and Nenes, 2014) rely on their estimates of CCN concentrations which are calculated based on simplified treatment of aerosol size distributions, chemical compositions and the Köhler theory leading to varying degrees of uncertainty depending on specific scheme used (Simpson et al., 2014). Enhanced understanding of aerosol particles and their role as CCN may be used to improve representations of aerosol-cloud interactions (ACI) in global climate models, which remain a significant source of uncertainty in estimates of total anthropogenic radiative forcing over the industrial period (IPCC report, 2021; Seinfeld et al., 2016).

N_{CCN} and CDNC are primarily determined by aerosol properties and the drivers of SS_{max} fluctuations (e.g. updraft velocities, radiative cooling rates, water vapor concentration field see e.g. Köhler, 1936; Rogers and Yau, 1989; Reutter et al., 2009; Anttila et al., 2012; Partridge et al., 2012), both of which are known to display large spatial and temporal variability. Many studies have evaluated N_{CCN} predictions from Köhler theory against observations of aerosol particle size distributions, chemical composition and meteorological parameters in various environments. These investigations, often termed aerosol-CCN closure studies or hygroscopicity-CCN closure studies, will be referred to here simply as 'closure studies'. Typically, such studies have involved forward modeling, where observational input data (e.g., aerosol size distribution, composition, and hygroscopicity) is utilized to predict N_{CCN} using a CCN prediction model. The model outputs are then compared directly with observed CCN data to assess consistency and evaluate the predictions (e.g., Bougiatioti et al., 2009; Martin et al., 2011; Rejano et al., 2024). However, relatively few studies have leveraged inverse modeling frameworks, which use observed CCN data to infer the properties of the aerosol population or model parameters. These inverse approaches allow for testing model assumptions and constraining observed CCN concentrations as a function of uncertain calibration parameters (e.g., Partridge et al., 2011, 2012; Lowe et al., 2016).

In earlier studies, Köhler theory (Köhler, 1936) was widely used as the standard framework for predicting CCN activation and proved effective under most relevant atmospheric conditions, provided that there was accurate knowledge of the aerosol number size distribution, size-dependent chemical composition, and *SS*. To simplify the representation of aerosol hygroscopic growth and CCN activity, Petters and Kreidenweis (2007) introduced the non-dimensional hygroscopicity parameter κ, to facilitate comparisons of data sets with varying levels of detail for the aerosol chemical composition. These theoretical frameworks along with information about particle number size distributions and chemical composition are utilized to calculate the activation diameter (D_{act}) of the dry particles and finally the CCN concentration at a particular ambient *SS*. A successful closure study aims for the modelled CCN and measured CCN to be comparable within measurement uncertainties and is notably influenced by the accuracy of the relevant measurements and any theoretical approximations.

https://doi.org/10.5194/egusphere-2025-1602
Preprint. Discussion started: 8 May 2025

The aqueous phase thermodynamics of soluble inorganic salts like ammonium sulfate ($(NH_4)_2SO_4$), sodium chloride (NaCl), ammonium bisulfate (NH_4HSO_4) and ammonium nitrate (NH_4NO_3) are considered to be relatively well-understood (e.g., Zhang et al., 2000 and Nenes et al., 1998, 1999), and yield accurate predictions of CCN activation of these compounds using Köhler theory. However, atmospheric aerosol particles also typically contain a significant organic mass fraction (Zhang et al., 2007), originating from various sources. In the atmosphere, organic aerosol typically forms a complex mixture with inorganic aerosol species. The organic component evolves over time modifying both the mass concentration and the properties of the aerosol (Robinson et al., 2007; Jimenez et al., 2009). Organic aerosol comprises of a wide variety of molecules (e.g., Hallquist et al., 2009; Nozière et al., 2015; Ditto et al., 2018) with different properties, such as solubility volatility and surface activity (e.g., Hodzic et al., 2014; Ye et al., 2016; Huang et al., 2024; Haber et al., 2024). While many of the atmospheric organic compounds are water-soluble, their hygroscopicity is typically lower than that of inorganic salts (e.g., Pöhlker et al., 2023). Still, organic aerosol plays a significant role in determining (N_{CCN}) and CDNC, especially because organic aerosol formation drives aerosol particle growth towards CCN-relevant sizes in many environments (e.g., Riipinen et al., 2011; Mohr et al., 2019; Croft et al., 2019; Zheng et al., 2020; Qiao et al., 2021). Importantly, some organic aerosol properties beyond hygroscopicity may enhance the likelihood of an Aitken mode aerosol particle to serve as CCN (Lowe et al., 2019). Historically, in studies where the organic aerosol contribution to the CCN activation was not adequately considered, errors of up to an order of magnitude were observed between predicted and measured N_{CCN} in many environments (e.g., Bigg et al., 1986; Covert et al., 1998; Chuang et al., 1999; Rissman et al., 2006; Quinn et al., 2008). This discrepancy highlights the need to include organics in CCN prediction models. Studies incorporating organic aerosol effects demonstrated significant improvements in closure as compared with attempts considering inorganics alone (e.g., Broekhuizen et al., 2006; Rose et al., 2008; Ervens et al., 2009; Guenther et al., 2009; Bougiatioti et al., 2009; Jurányi et al., 2010). These findings underscore the importance of organics in CCN prediction, particularly in air masses with substantial freshly emitted primary biogenic or anthropogenic organic vapors.

Boreal forests are environments where local biogenic emissions act as a major source of aerosol particles, organic aerosol constituting 50-80% of the observed sub-micron aerosol mass (Heikkinen et al., 2020). This dominance of organics results from the emission of biogenic volatile organic compounds (BVOCs) by the forests, which promotes secondary organic aerosol (SOA) production. Understanding the factors controlling N_{CCN} above boreal forests is necessary for constraining the magnitude of the climate feedbacks involving natural forest aerosols and clouds which are likely to increase in importance as anthropogenic aerosol emissions decrease (see e.g., Paasonen et al., 2013; Yli-Juuti et al., 2021; Blichner et al., 2024).

Hämeri et al. (2001) utilized Hygroscopicity Tandem Differential Mobility Analyzers (HTDMAs) during the BIOFOR campaign at the SMEAR II Hyytiälä forest field station in south-central Finland, to measure the hygroscopic growth factors of aerosol particles at 90% relative humidity (RH), and reported Aitken mode particles (with growth factors between 1.0 and 1.4) to be less hygroscopic than accumulation mode particles (growth factors ~ 1.6). Sihto et al. (2011) studied the annual cycles of aerosol hygroscopicity and CCN, finding the hygroscopicity at sub-saturated conditions to be a good predictor of the CCN activity as well. They concluded the average hygroscopicity parameter κ to be 0.18 (for *SS* values between 0.1 and 1 % during Jul 2008 and Jun 2009) and therefore, the CCN-sized particles to be mostly organic, but to also contain more hygroscopic material such as ammonium sulfate (see also Cerully et al., 2011). Paramonov et al. (2013) used a size-segregated CCN observation

https://doi.org/10.5194/egusphere-2025-1602
Preprint. Discussion started: 8 May 2025

data set collected between January 2009 and April 2012 from Hyytiälä, which revealed that the median κ exhibited significant variation depending on the *SS* and hence particle size. Specifically, median κ was 0.41 at a *SS* of 0.1% (corresponding to larger activation dry diameter) 0.14 at a *SS* of 1.0% (corresponding to smaller activation dry diameter), where the upper end represents a primarily inorganic aerosol and the lower end organic dominance. The size-dependence of hygroscopicity was more pronounced during the winter months compared to the summer. In a follow-up study, Paramonov et al. (2015) identified a statistically significant difference in the hygroscopicity of Aitken and accumulation mode particles in northern locations and concluded that the assumption of a size-independent κ potentially leads to a systematic overprediction in CCN predictions at supersaturations above 0.6% in the boreal environment. In the closure study by Schmale et al. (2017), predictions using bulk chemical composition data indeed led to an over-prediction (geometric mean bias of 1.32 at SS = 0.5%) of N_{CCN} for the period between Jan 2012 and Jun 2014.

In large-scale atmospheric models, the aerosol size distribution is often represented by a number of log-normal modes, and N_{CCN} are estimated from SS_{max} based on dynamics (e.g., updraft) and physicochemical properties of the aerosol modes – as the abundance of particles with variable sizes and compositions influences the development of *SS* and hence the CCN activation (e.g., Abdul-Razzak and Ghan, 2000). A number of studies (e.g., Sihto et al., 2011; Paramonov et al., 2013; 2015; Bulatovic et al., 2021; Pöhlker et al., 2021; Lowe et al., 2019, and Duplessis et al., 2023) have demonstrated that Aitken mode particles can contribute significantly to CDNC, particularly in clean conditions. Therefore, constraints for the physicochemical properties of both Aitken and accumulation mode particles are important for predictions of N_{CCN} and CDNC. Unfortunately, the standard methods used for measurements of aerosol chemical composition (e.g., Aerosol Chemical Speciation Monitor ACSM; see Sect. 2.1.4) cannot typically separate accumulation and Aitken mode composition. The few studies reporting size-segregated aerosol composition in forested environments suggest an enrichment of inorganics in the accumulation mode, and higher mass fractions of organics in the Aitken mode (Allan et al., 2006; Hao et al., 2013; Levin et al., 2014; Timonen et al., 2008; Saliba et al., 2020). Studies involving a full annual coverage suggest a more size-dependent composition in early spring and winter (Levin et al., 2014; Timonen et al., 2008) compared to the summer. These findings are also qualitatively in line with the studies investigating the growth of Aitken mode particles in Hyytiälä, explainable with organic condensation (e.g., Riipinen et al., 2011 Mohr et al., 2019). Campaign-wise studies like Cubison et al. (2008); Broekhuizen et al. (2006); Stroud et al. (2007); Meng et al. (2014) used size-resolved Aerosol Mass Spectrometer (AMS) data, which is typically sparse, to achieve CCN closure in different environments, demonstrating that size-dependent chemical composition of aerosol particles can often explain the apparent discrepancies between observed and predicted CCN concentrations. Taken together, these results suggest that observations of CCN concentrations have the potential to be used in an inverse manner to constrain Aitken and accumulation mode chemical compositions separately – if information on the particle size distribution and an estimate of the bulk chemical composition is available.

In this study, we employ long-term (2016–2020) concurrent measurements from the SMEAR II atmospheric monitoring site in the boreal forest (Hyytiälä, Finland) to perform an inverse aerosol-CCN closure. Additionally, we test the performance of two forward closure approaches: a commonly used approach, which utilizes the bulk aerosol chemical composition (i.e., size-independent composition) observations ('bottom-up' approach) to estimate the hygroscopicity parameter κ and predict CCN concentrations, and a simpler approach

https://doi.org/10.5194/egusphere-2025-1602
Preprint. Discussion started: 8 May 2025

using a constant hygroscopicity value of 0.18 throughout the study period, as recommended by Sihto et al. (2011). Specifically, our study aims to address the following questions:

1. How does the chosen representation of κ affect the CCN closure on a multi-year and seasonal basis?
2. To what degree can a forward CCN closure be achieved when assuming size-independent chemical composition?
3. Can we improve CCN closure by assuming mode-dependent composition while keeping the size distribution fixed to the observations?
4. What modal chemical composition and κ yield a more accurate closure compared to using bulk chemical composition?

2 Methods and data

Figure 1 provides an overview of the data and approach used in this study. The core long-term data sets utilized were simultaneous observations of aerosol number size distribution between 3 and 1000 nm, chemical composition of the sub-micron (bulk) aerosol fraction and N_{CCN} at SS between 0.1% and 1% during the period of 2016 – 2020. κ-Köhler theory (Petters and Kreidenweis, 2007) was used to predict N_{CCN} based on the size distribution and composition data with three different approaches for estimating the hygroscopicity parameter κ: (1) κ_{bulk}, i.e. calculating κ using the observed bulk (size-independent) sub-micron aerosol composition; (2) $\kappa_{0.18}$, i.e. using a constant κ value of 0.18 (Sihto et al., 2011) for the entire observation period; and 3) κ_{opt} , i.e. determining κ through an inverse closure assuming variable Aitken and accumulation mode compositions while maintaining the total sub-micron chemical composition as observed.

In the following subsections we present further details on the measurement site and observations of aerosol number size distribution, sub-micron chemical composition, as well as concentrations of CCN at different supersaturations. Finally, a detailed description of methods including κ-Köhler theory and inverse closure is provided.

https://doi.org/10.5194/egusphere-2025-1602
Preprint. Discussion started: 8 May 2025

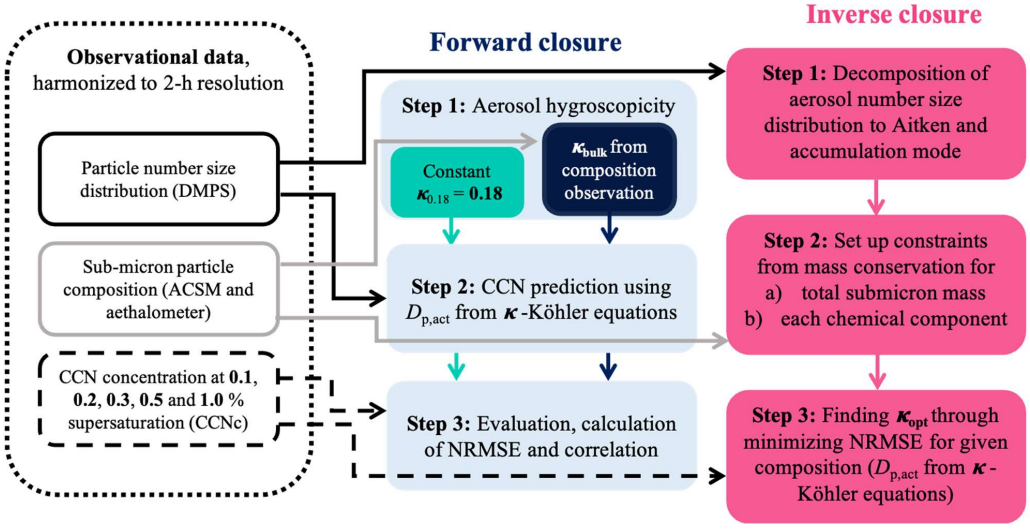

Figure 1: Workflow diagram of the observational data along with the steps made in its processing and analysis. NRMSE and $D_{p,act}$ refer to Normalized Root Mean Squared Error (see Sect. 2.2.4) and dry activation diameter respectively. DMPS refers to Differential Mobility Particle Sizer, ACSM to Aerosol Chemical Speciation Monitor, CCN to Cloud Condensation Nuclei and CCNc to Cloud Condensation Nuclei counter.

2.1 Experimental data

2.1.1 Station for Measuring Ecosystem–Atmosphere Relations (SMEAR II)

The SMEAR II measurement site at Hyytiälä is located at 61° 51′ N, 24° 17′ E, 181 m above sea level, and represents a boreal forest environment with some anthropogenic influence, particularly from the southern direction where many industrialized areas within Finland, Russia, and continental Europe are located (Patokoski et al., 2015; Riuttanen et al., 2013; Yttri et al., 2011; Tunved et al., 2006). The station is surrounded by mixed forest which covers 80% of the land within a 5 km radius and 65% within a 50 km radius (Williams et al., 2011) and one of the primary local emission sources includes a sawmill situated to the northeast and a pellet factory located around 6–7 km southeast of SMEAR II. The station can be considered a rural background site because the nearest major city, Tampere, is located about 60 km southeast of the measurement location. During the summer, local BVOC emissions (Hakola et al., 2012; Barreira et al., 2017), primarily those of monoterpenes, act as a major source of SOA at the station (Heikkinen et al., 2020; Heikkinen et al., 2021). New particle formation (NPF), that is an important process contributing to N_{CCN} globally (e.g., Merikanto et al., 2009), is commonly observed at SMEAR II, especially in spring and fall (Nieminen et al., 2014). Sulfuric acid, bases and low-volatility BVOC oxidation products (e.g., Kulmala et al., 2014; Lehtipalo et al., 2018; Yan et al., 2018), have been identified as critical precursors for NPF at the site. During the winter, aerosol particles observed at the site are mainly long-range transported (Riuttanen et al. 2013) and frequently cloud-processed (Isokääntä et al. 2022). During this season, aerosol particles contain a larger inorganic component (Heikkinen et al., 2020) increasing their hygroscopicity. However during the winter time more black carbon is also observed (Luoma et al., 2019), which

https://doi.org/10.5194/egusphere-2025-1602
Preprint. Discussion started: 8 May 2025

´tends to decrease the overall hygroscopicity. SMEAR II is unique due to the comprehensive set of long-term measurements, crucial for answering questions related to aerosol-cloud interactions, which have been conducted for several years (Kulmala, 2018). Although facilities for measuring aerosol size distribution and CCN have existed for a long time (since 1996 and 1998, respectively), long-term composition measurements have become available more recently (Luoma et al., 2021; Heikkinen et al., 2020). This advancement has been due to the development and deployment of the ACSM and an aethalometer setup which provide near-real time data on the organics, sulfate, nitrate, ammonium, chloride and equivalent black carbon (eBC) in sub-micrometre aerosol particles (Sect. 2.1.4).

2.1.2 Aerosol number size distribution

At SMEAR II, a Differential mobility Particle Sizer (DMPS) has been used for particle number size distribution (PNSD) measurements in a size range from 3 nm to 1000 nm since 1996 (Aalto et al. 2001). The DMPS data has the time resolution of 10 minutes. The data were accessed from SmartSMEAR database (https://smear.avaa.csc.fi/download) for years 2016–2020 (see Fig. 2a). Medians of the size distribution data were taken over the start and end time periods in the respective co-located CCN measurements (see Sect. 2.1.3).

The twin-DMPS system consists of two Vienna-type Differential Mobility Analyzers (DMAs), each designed to classify aerosol particles into size bins across two distinct size ranges: 3-40 nm and 20-1000 nm. The sizing is based on the electrical mobility of the sampled and charged aerosol particles. Air is sampled at a height of 8 meters above ground level with a common aerosol inlet. The common inlet line has a diameter of 100 mm and a flow velocity of 0.5 m s^{-1}. The sample flow for the instruments is taken from the centreline. The aerosol flow rates in the DMAs are 4 L min^{-1} and 1 L min^{-1}, respectively. The sheath flows, with flow rates of 20 L min^{-1} and 5 L min^{-1}, are dried to maintain RH of less than 40%, while the aerosol flows are not dried. The particle concentration following each DMA is measured using Condensation Particle Counters (CPCs). For small particles (3–40 nm), a TSI 3025 CPC model was utilized (later changed to model TSI3776 after October 2016), while a TSI 3750 CPC is used for the detection of the larger particles in the size range 20–1000 nm.

For the inverse closure, we used a Python version (Khadir, 2023) of the algorithm by Hussein et al. (2005) to fit two modes into the measured aerosol size distributions. The algorithm takes size distribution as input and returns the lognormal parameters (number concentration, geometric standard deviation, geometric mean diameter) of different modes as output. While the algorithm would allow fitting up to four modes, bimodal fits (Aitken and accumulation mode, respectively; Fig. S1a) were selected to avoid overfitting. The bimodal fits enabled us to reproduce the aerosol size distributions with a high correlation (pearson correlation coefficient = 0.99) between the observed total particle number concentration and that calculated from the fitted parameters (see Fig. S1b).

2.1.3 CCN concentrations

The time series of observed N_{CCN} were obtained using a CCN-100, a continuous-flow streamwise thermal-gradient CCN counter (CCNc), commercially provided by Droplet Measurement Technologies (Roberts and Nenes, 2005). The CCNc can be used in either monodisperse or polydisperse mode, where the former is utilized to determine size-segregated N_{CCN}, as detailed in Paramonov et al. (2013). In contrast, the polydisperse mode, employed here, measures the overall N_{CCN} at a given supersaturation.

https://doi.org/10.5194/egusphere-2025-1602
Preprint. Discussion started: 8 May 2025

The CCNc consists of a saturator unit and an Optical Particle Counter (OPC). The saturator includes a vertical flow tube where aerosol samples are introduced alongside filtered sheath air under laminar flow conditions, creating a central flow path. The tube's inner surface is kept moist to generate a supersaturation gradient. As the laminar flow moves through the column, heat and water vapor move from the tube's inner walls towards the center. Due to the faster diffusion of water molecules compared to heat, a stable water vapor supersaturation is maintained along the tube's centerline. The effective supersaturation is influenced by factors such as flow rate, pressure, and temperature gradient. While moving through the tube, aerosol particles absorb water and grow and those particles with critical supersaturations lower than the centerline supersaturation are activated as cloud droplets. Droplets larger than 0.75 µm in diameter are detected by the OPC at the exit of the tube and those exceeding 1 µm are considered to be activated CCN. To measure at different supersaturations, the temperature gradient is increased in steps while the flow rate is constant. Quantification and discussion of typical uncertainties related to the supersaturation and hence N_{CCN} measured with this instrument are presented in e.g., Rose et al. (2008) and Topping (2005). At SMEAR II, the air to CCNc is sampled 8 meters above the ground level and features an inlet same as in DMPS (see Sect. 2.1.3.). The aerosol flow rate is 0.5 L min^{-1}, which is split into sheath flow of 0.45 L min^{-1} and sample flow of 0.045 L min^{-1}. For quality assurance of the CCNc data, the CCNc calibration is conducted approximately twice a year using nebulised, dried, charge equilibrated and size-segregated ammonium sulfate aerosol following procedure as per Rose et al. (2008).

Estimates of smallest activation dry diameter (D_{act}) were derived using the combination of the DMPS and the CCNc data by integrating the particle number size distributions from their maximum diameters to the diameter at which the integrated particle number was equal to the measured N_{CCN}. D_{act} was then calculated by interpolating between the two adjacent size bins (Furutani et al., 2008). Essentially, variations in activation diameter reflect differences in the chemical composition of aerosol particles: the more hygroscopic the aerosol, the smaller the activation diameter.

2.1.4 Aerosol chemical composition

An Aerosol Chemical Speciation Monitor (ACSM; Ng et al., 2011) was used to retrieve long-term observations of the non-refractory sub-micron particulate matter (NR-PM_1; i.e., organics, sulfate, nitrate, ammonium and chloride) at SMEAR II. Briefly, the ACSM samples dried ambient air through a critical orifice (100 µm in diameter) with a flow rate of 1.4 cm^3 s^{-1} to an aerodynamic lens (Liu et al. 1995a; Liu et al. 1995b), which focuses a submicron particle beam and directs it to the instrument vaporization and ionization chamber. The lens efficiently transmits particles with vacuum aerodynamic diameters (D_{va}) ranging from approximately 75 to 650 nm, yet it also passes through particles up to 1 µm in D_{va} with a less efficient transmission. These aerosol particles then undergo flash vaporization at 600 °C and are subsequently ionized using electron impact ionization (70 eV) and the mass spectrum is obtained with quadrupole mass spectrometry. While the vacuum system of the ACSM efficiently reduces the amount of air molecules entering the instrument detection unit, their distinction from the aerosol components is required. For this purpose, the ACSM contains a 3-way valve system to routinely measure the signals obtained from particle-free air, and this background is subtracted from the particle-laden sample. The detailed description of the ACSM measurements performed at SMEAR II since 2012 is provided in Heikkinen et al. (2020), which includes descriptions of the instrument ionization efficiency calibrations, collection efficiency corrections and data processing. The ACSM measurements were conducted < 100 m away from the DMPS, CCNc

https://doi.org/10.5194/egusphere-2025-1602
Preprint. Discussion started: 8 May 2025

and aethalometer measurements in a separate container. A $PM_{2.5}$ cyclone was installed to the container roof, and the ~3 m long inlet line had an additional make-up flow of 3 L m^{-1}. The air was dried to < 30% RH with a Nafion dryer. The original time resolution of the ACSM data is ~30 minutes.

We combined the ACSM measurements with measurements of equivalent Black Carbon (eBC). The eBC concentration was determined based on PM light absorption measured by an aethalometer (Magee Scientific, models AE31 and AE33). For the period in question here (2016-2020), the instrument was changed in the middle as the old instrument broke down. AE31 operated until the end of 2017 and AE33 started measuring in the beginning of 2018. Aethalometer is a filter-based instrument and it measures aerosol light absorption at seven wavelengths (370, 470, 520, 590, 660, 880, and 950 nm). To consider the measurement artefacts in the measurements caused by collecting the particles in a filter medium, the aethalometer data were corrected for the so-called loading effect and scattering caused by the filter material: AE33 applied the inbuilt dual-spot correction (Drinovec et al., 2015) with multiple scattering correction factor 1.39 whereas the AE31 data were corrected as suggested by Virkkula et al., 2007 with multiple scattering correction factor 3.14 (derived by Luoma et al., 2021 for SMEAR II data). The eBC concentration was derived from the absorption at 880 nm channel by using mass absorption cross-section of 7.77 g m^{-2} for AE33 data (the default value suggested by the manufacturer) and 4.8 g m^{-2} for AE31 data (derived from 6.6 g m^{-2} at 637 nm used for multi-angle absorption photometer, which was used as a reference in Luoma et al., 2021). The head of the sampling line was located 4 m above the ground. The concentration of eBC was measured for PM_{10}. Sample air was dried with by a Nafion dryer and data was marked as invalid, if the relative humidity inside the instrument increased above 40%. The aethalometer data was converted to STP conditions (273.15 K, 1013.25 hPa).

The published ACSM and eBC measurements data are averaged over 1-hour intervals, but to concur with the CCN measurement, the data set was further converted to the 2-hour time grid by taking a median of the mass concentrations of each of the measured species over the time window of each CCN measurements. The time series (7-day running median) are shown in Fig. 2b. The data coverage is higher for the eBC data compared to the ACSM data, which has fewer observations during wintertime.

2.1.4 Data coverage and seasonal classification

Figure 2 presents the overall data coverage along with the key aerosol properties observed (see Fig. S2 for the number of data points across different seasons). As mentioned earlier, SOA formation and NPF events lead to higher particle number concentrations during spring and summer. This is also reflected in the variability of CCN, particularly at higher supersaturations (see Fig. 2b), while lower seasonal variation is observed at lower supersaturations (SS = 0.1%), where only larger particles (> 200 nm, see Fig. S3) are activated. This suggests that most changes in aerosol particle number and chemical composition occur among smaller particles (Aitken and nucleation modes) between the winter and growing seasons (spring and summer). In terms of chemical composition, organics dominate the aerosol mass (see Fig. 2c), especially during the growing seasons, followed by sulfate and ammonium ions, with nitrate and black carbon contributing only minor fractions. However, given the significant seasonal variation in overall aerosol properties at the site, we present the results according to a seasonal classification. In this framework, March, April, and May represent spring; June, July, and August represent summer; September, October, and November correspond to autumn; and December, January, and February correspond to winter.

https://doi.org/10.5194/egusphere-2025-1602
Preprint. Discussion started: 8 May 2025

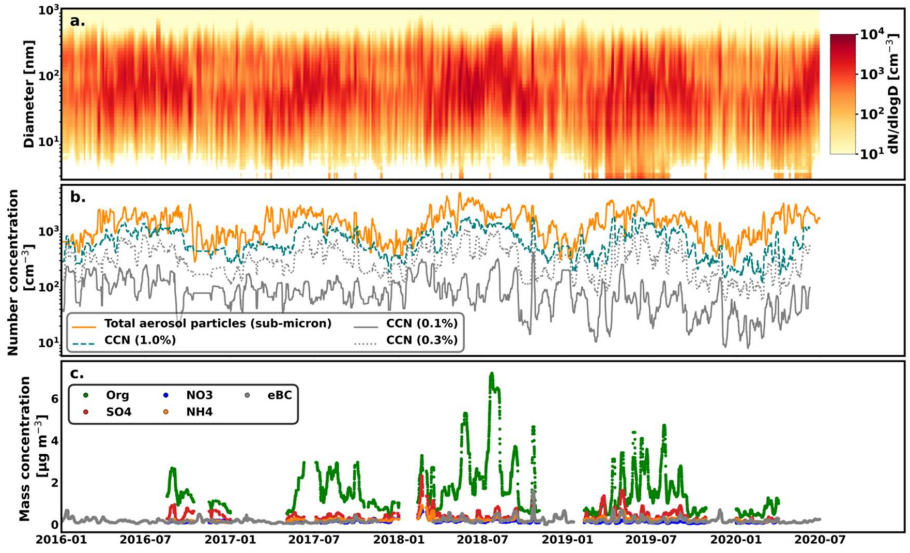

Figure 2: Temporal coverage of the observation data represented through seven-day running median. The top panel (a) shows the variation of the aerosol size distribution. The middle panel (b) shows the total number concentration of sub-micron aerosol particles (in orange) and CCN at 0.1, 0.3 and 1.0% supersaturation (in grey). The bottom panel (c) presents the mass concentrations of various chemical species and ions in the aerosol particles: organics (Org), sulfate (SO_4), nitrate (NO_3), ammonium (NH_4), and equivalent black carbon (eBC).

2.2 Calculations for the forward and inverse closure studies

2.2.1 κ-Köhler theory

The classical Köhler theory (Köhler, 1936) utilizes information about the composition and size of aerosol particles. It estimates the critical supersaturation level SS_{crit} and wet particle diameter at which an aerosol particle becomes activated and grows through condensation to form a cloud droplet. The Köhler equation comprises two terms (see Eq. 1): one accounting for the influence of solutes (the soluble fraction of aerosol particles), which tends to reduce the equilibrium saturation ratio S (defined as 1 + SS), and the other known as the Kelvin term, which represents the increased surface tension over a spherical surface. In an aqueous solution, if P (Pa) is the partial vapor pressure of water and P_s (Pa) saturation vapor pressure of water over a pure flat liquid, the equilibrium saturation ratio $S = P/P_s$ is represented as

$$S = a_w \exp\left(\frac{4\sigma M_w}{RT\rho D_{p,wet}}\right) \quad (1)$$

where a_w is the activity of water in the solution, ρ is the density of the solution (kg m^{-3}), M_w is the molecular weight of water (0.018 kg mol^{-1}), σ (N m^{-1}) is the surface tension of the solution, R is the universal gas constant (8.314 J mol^{-1} K^{-1}), T is temperature (K), and $D_{p,wet}$ is the diameter of the droplet (m). To facilitate the comparison

https://doi.org/10.5194/egusphere-2025-1602
Preprint. Discussion started: 8 May 2025

to previous work, we use the modified version of Köhler theory (Eq. 1) described by Petters and Kreidenweis (2007) to calculate the activation dry diameter (related to the total amount of soluble mass) for a particular supersaturation SS (i.e., $S - 1$) and termed as the κ-Köhler framework

$$S = \frac{D_{p,wet}^3 - D_{p,dry}^3}{D_{p,wet}^3 - D_{p,dry}^3 (1-\kappa)} \exp\left(\frac{4\sigma M_w}{RT\rho D_{p,wet}}\right) \quad (2)$$

where $D_{p,dry}$ is the dry diameter of the dry aerosol particle (m) with a given composition described by a unitless hygroscopicity parameter κ. In our calculations, we have assumed that the density and surface tension of the solution are equivalent to those of water (1000 kg m^{-3} and 0.0728 N m^{-1} respectively). Additionally, we have considered a constant ambient temperature (T) of 298.48 K for all seasons, corresponding to the median temperature inside the measurement hut.

Assuming internally mixed aerosol particles, the net hygroscopicity parameter κ for a mixture of n different chemical species is expressed as the linear combination of the individual species κ_i weighted by their respective volume fractions ε_i in the dry particle (Stokes and Robinson, 1966):

$$\kappa = \sum_i \varepsilon_i \kappa_i \quad (3)$$

The volume fractions ε_i of the individual components were calculated from the measured mass concentrations, m_i, and their respective densities, ρ_i

$$\varepsilon_i = \frac{\frac{m_i}{\rho_i}}{\sum \frac{m_i}{\rho_i}} \quad (4)$$

2.2.2 Forward closure

In the forward closure, N_{CCN} at supersaturations of 0.1%, 0.2%, 0.3%, 0.5%, and 1.0% (corresponding to the supersaturations set in the CCNc, henceforth referred to as SS_{CCNc}) are predicted using observations of the aerosol number size distribution from the DMPS. As discussed above (see Sect. 2), two different assumptions about the hygroscopicity of the aerosol mixture were tested: 1) Assuming constant hygroscopicity of 0.18 ($\kappa_{0.18}$) 2) Assuming mixture hygroscopicity (Eq. 4) using chemical composition information from the ACSM and aethalometer measurements (κ_{bulk}). κ_{bulk} therefore, does not depend on particle size, but is variable in time. For deriving κ_{bulk} the observed aerosol chemical composition was utilized, assuming that all sulfates are present as ammonium sulfate $(NH_4)_2SO_4$ (AS) and the observed nitrate was distributed between ammonium nitrate NH_4NO_3 (AN) and organic nitrate (ON) was estimated using the method (Supplementary note 1 and Fig. S4 for details) explained in Farmer et al. (2010). For the calculation of the AS and AN mass concentration, only the measured sulfate and nitrate mass concentrations were used. The ammonium mass concentration required for yielding ion balance within the particles was calculated (see Fig. S5; Zhang et al., 2007). We acknowledge that the assumption that sulfate is present solely as AS can cause underestimations of aerosol hygroscopicity at SMEAR II, because

https://doi.org/10.5194/egusphere-2025-1602
Preprint. Discussion started: 8 May 2025

aerosols can be more acidic at the site (e.g., Riva et al., 2019). Finally, to retrieve the volume fractions of organics, AS, AN, ON and eBC from their estimated mass concentrations, the density information for each species is required. The chosen densities are shown in Table 1 along with the κ_i for each species.

Table 1. Densities (ρ_i) and hygroscopicity parameters (κ_i) of the assumed dry particle constituents based on the composition estimated from the ACSM and the aethalometer measurements.

Species	ρ (kg m^{-3})	κ
Organics	1500 (Kostenidou et al., 2007)[a]	0.12 (Pöhlker et al., 2023)
Ammonium nitrate (AN)	1720	0.67 (Petters and Kreidenweis, 2007)
Ammonium sulfate (AS)	1769	0.61 (Petters and Kreidenweis, 2007)
Organic nitrate (ON)	1500[b]	0.12[b]
Equivalent black carbon (eBC)	1770 (Park et al., 2013)	0 (Weingartner et al., 1997)

[a]SOA density estimated to be in the 1400 – 1650 kg m^{-3} range when formed from BVOCs known to produce the majority of SOA at SMEAR II. 1500 kg m^{-3} is chosen from this range.
[b]Set to equal that of the rest of the organics for simplicity. Some studies suggest that the density could be slightly lower (1160 – 1210 kg m^{-3}, Claflin et al., 2018).

The critical supersaturation SS_{crit} was then calculated for each of the size bins measured by the DMPS using the κ-Köhler theory, assuming a uniform composition throughout the size distribution. Particles for which the calculated SS_{crit} was lower than the individual SS_{CCNc} were then considered as CCN corresponding to the respective SS_{CCNc} value. Linear interpolation was applied to estimate the exact activation diameter within a given size bin (see Lowe et al., 2016). The CCN spectra estimated by the forward closure were then compared to the observations made by the CCNc for the two different hygroscopicity assumptions i.e. κ_{bulk} and $\kappa_{0.18}$.

2.2.3 Inverse closure

In the inverse closure, our objective is to minimize the Normalized Root Mean Squared Error (NRMSE, see Sect. 2.2.4) between predicted and observed N_{CCN}, while optimizing the hygroscopicity parameter (denoted κ_{opt}). This makes κ_{opt} variable in time as well as a function of particle size. More specifically, the size-dependency of κ_{opt} is approximated by assuming the size distribution to consist of two internally mixed log-normally spaced aerosol modes, specifically the Aitken or accumulation mode. Importantly, for the κ_{opt} derivation, all AN and AS masses were combined and treated as inorganic mass for simplicity. The net ρ and κ of the inorganic fraction were derived using the corresponding observed mass fraction. While the κ for AN is slightly higher than that of AS (Table 1) and the density of AN is slightly lower of that of AS (Table 1), we consider this as a reasonable simplification given the low AN concentration at the site. Again, all ON is assumed to have the same κ and ρ as the organics (Table 1). Another important simplification concerns eBC, which is assumed to have the same mass fraction in both the Aitken and accumulation modes. Attaining of κ_{opt} starts by a bimodal fitting of the aerosol number size distribution to the Aitken and accumulation modes (see Sect. 2.1.2). Next, the fitted lognormal parameters of size distributions were used to produce the fitted aerosol number size distribution binned onto the same diameter axes

https://doi.org/10.5194/egusphere-2025-1602
Preprint. Discussion started: 8 May 2025

as the observational data, and the number of particles in each bin was scaled to match the particle number in measured size distribution (see a demonstration in Fig. S6 and Supplementary note 2). This way, the number contributions of the Aitken and accumulation modes to the observed aerosol size distribution could be estimated for each time point. Second, the masses of both the Aitken and accumulation modes were estimated using the assumptions outlined above, and approximating the density of both modes by the bulk density. The total masses of organics, inorganics and eBC to be distributed to the measured size distribution are then calculated using the mass fractions derived from the ACSM and aethalometer measurement. Finally, the Aitken vs. accumulation mode compositions, and hence κ_{opt}, fulfilling these constraints and best reproducing the observed CCN spectra were found through optimization.

2.2.4 Metrics for assessing the goodness of closure

The optimization described above was done by minimizing the NRMSE between the observed CCN spectra and the calculated CCN spectra (taken as the sum of the Aitken and accumulation mode CCN spectra) by implementing the Nelder-Mead optimization algorithm (Gao and Han 2012) available in the Python SciPy library. The Nelder-Mead algorithm is a widely used optimization method that iteratively searches for the minimum or maximum of an objective function. The optimization goal was to determine the optimal modal chemical composition in terms of mass fractions of different species (see supplementary note 3 and Fig. S7) and eventually the hygroscopicity (κ_{opt}) that minimized the Normalized Root Mean Square Error (NRMSE) between observed and predicted CCN concentrations. The NRMSE was calculated for as:

$$\mathrm{NRMSE} = \frac{\sqrt{\frac{1}{n}\sum_{i=1}^{n}(\mathrm{CCN}_{\mathrm{pred},i} - \mathrm{CCN}_{\mathrm{obs},i})^2}}{\overline{\mathrm{CCN}_{\mathrm{obs}}}} \quad (5)$$

Where $\mathrm{CCN}_{\mathrm{pred},i}$ is the predicted CCN concentration at supersaturation i, $\mathrm{CCN}_{\mathrm{obs},i}$ is the observed CCN concentration at supersaturation i, n is the number of data points (in this case five, as we have five different supersaturations) and $\overline{\mathrm{CCN}_{\mathrm{obs}}}$ is the mean of the observed CCN concentrations across all supersaturations. To facilitate direct comparison with Schmale et al. (2016) we also calculated the Geometric Mean Bias (GMB) for each time point, defined as:

$$\mathrm{GMB} = \exp\left(\frac{1}{n}\sum_{i=1}^{n}\ln\left(\frac{\mathrm{CCN}_{\mathrm{pred},i}}{\mathrm{CCN}_{\mathrm{obs},i}}\right)\right) \quad (6)$$

3 Results and discussion

3.1 Size distributions and activation diameters

Figure 3 presents the median and quartiles of lognormal aerosol number size distributions and median activation diameters (D_{act}) calculated from the PNSD-CCN closure across different seasons (see also Supplementary note 2). The shape of a lognormal size distribution depends on the age of the aerosol population, and the atmospheric processing (e.g. nucleation, coagulation, condensation, deposition and chemical reactions) that has taken place

https://doi.org/10.5194/egusphere-2025-1602
Preprint. Discussion started: 8 May 2025

along the transport trajectory to the measurement site. As discussed previously (Sect. 1), freshly formed particles via NPF in spring (Nieminen et al., 2014) and at the same time, the temperature-dependent emissions of BVOCs leading to the formation of SOA (Heikkinen et al., 2020) result in bell-shaped size distributions with high particle number concentrations. In autumn and winter, on the other hand, biogenic aerosol precursor emissions are reduced leading to a lowering in the organic aerosol mass fraction. The contribution from long-range cloud-processed and aged particles increases, detected in the form of bimodal aerosol size distributions with predominant Hoppel minima (Hoppel et al., 1986) at around 80–90 nm in diameter, and increased inorganic aerosol mass fractions. The activation diameters decrease with increasing supersaturation and when all seasons are taken into account, median D_{act} (see Table S1) being generally higher than reported in earlier studies using similar methodology (e.g., Sihto et al., 2011; Paramonov et al., 2015). This could reflect decreasing abundance of sulfate during the last two decades as compared with less hygroscopic organic species (Fig. S8; see also Li et al., 2024). The activation diameters are relatively similar across the seasons (see Table S1), therefore suggesting a similar composition of the CCN over the year in comparison with the variability in the number size distribution. The slope of the particle number size distribution function is typically steep over the ranges of D_{act} corresponding to the investigated supersaturations. This indicates a high sensitivity of CCN to any parameters driving the particle number size distributions (see e.g., Lowe et al., 2016). While the median activation diameters show almost no seasonality, looking in more detail (see Fig. S4), an increase in the D_{act} is observed during the transition from winter to spring. This is probably due to the addition of more organic aerosol, which is less hygroscopic than the common inorganic salts. D_{act} reaches its maximum in summer and decreases again towards autumn. After autumn, there is an increase in D_{act} toward winter, despite a decrease in BVOC emissions and the resulting lower organic mass fraction alongside a higher inorganic fraction (see Fig. S9). This suggests the influence of another factor, possibly the higher eBC fraction observed during winter (see Sect. 3.3).

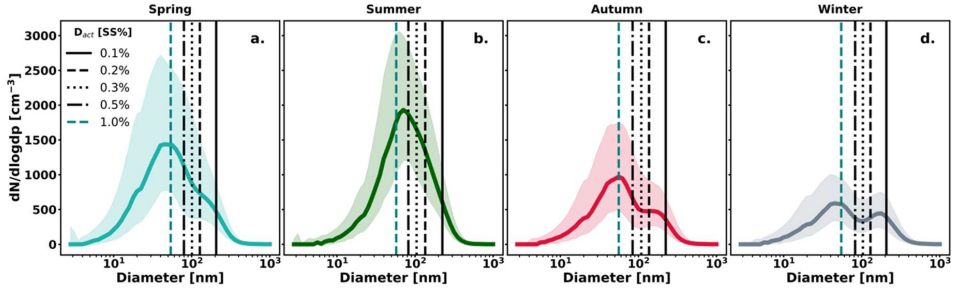

Figure 3: Seasonal overview of the lognormal size distribution, with solid lines representing the median and shaded regions indicating the interquartile range. The vertical lines denote the activation diameters (D_{act}) at various supersaturations as determined by combining the CCN data with the number size distribution measurements from the DMPS.

3.2 CCN spectra – Insights from forward and inverse CCN closures

Figure 4 shows the comparison between the observed and predicted CCN spectra, again displayed for each season separately. First, seasonal variations are evident, with CCN concentrations peaking in the summer and having their minimum in winter – in line with the overall particle number concentrations (see Fig. 3 and S9). The median

https://doi.org/10.5194/egusphere-2025-1602
Preprint. Discussion started: 8 May 2025

seasonal CCN concentration range from 29-76 cm^{-3} for 0.1% supersaturation, 101-317 cm^{-3} for 0.2%, 143-512 cm^{-3} for 0.3%, 170-744 cm^{-3} for 0.5%, and 300-1116 cm^{-3} for 1.0% with significant variations across seasons (Fig. 4 and Fig. S10). These values are somewhat lower than previous studies (Sihto et al., 2011; Paramonov et al., 2015), potentially related to decreases in overall particle number concentrations and a more prominent role of biogenic organic aerosols vs. inorganic sulfate (see e.g., Li et al., 2024) – also generally in line with the higher activation diameters reported here as compared to the previous studies. The NRMSE values for the forward closure between the predictions and the observations range from 0.49 to 0.94 (Table 2). The agreement of the forward closure is best for supersaturations of 0.2% and 0.3% where the activation diameter is generally within the accumulation mode range and hence also the ACSM composition is probably a more accurate estimate of the composition of the dry particles. The agreement is worst for the lowest supersaturation of 0.1 %, as also observed previously in Wang et al. (2010) and Meng et al. (2014). Furthermore, the agreement is better during spring and summer compared to autumn and winter. Interestingly, when comparing the results from the forward closures, a better closure is obtained with the simple constant value of $\kappa_{0.18}$ than with the "bottom-up" hygroscopicity estimate using the ACSM and aethalometer data (κ_{bulk}), indicating that assuming size-independent but temporally varying composition performs worse than a much simpler assumption. The results from the inverse closure (κ_{opt}), however, show that this issue can – at least to some degree – be mitigated when distributing the measured/estimated inorganic and organic species between the Aitken and accumulation modes. All methods (both the forward and inverse closures) tend to overpredict CCN numbers, with κ_{bulk} exhibiting the highest error.

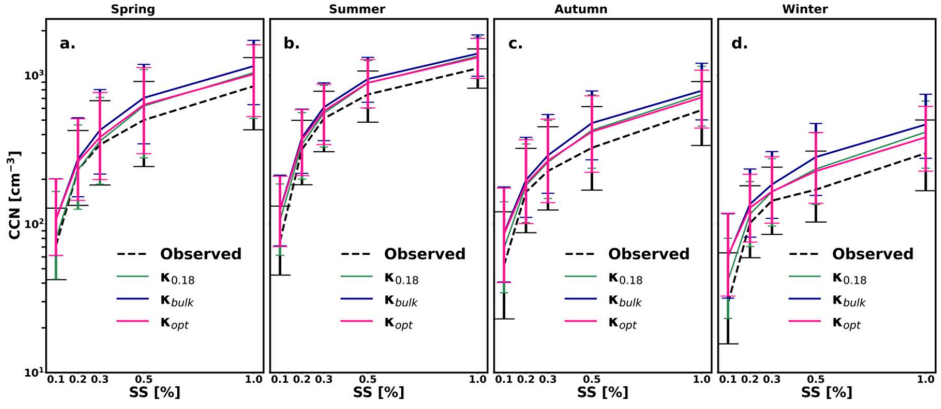

Figure 4: Observed (dashed) and predicted (solid) median CCN spectra in different seasons. The whiskers display the 25th and 75th percentiles.

When combined across all *SS* the overall NRMSE values for the entire timeseries are 0.43 for κ_{bulk}, 0.35 for $\kappa_{0.18}$ and 0.28 for κ_{opt}. To provide a more detailed perspective, we also calculated the NRMSE for each SS individually. Figure 5 provides an overview of how the three different methods perform in estimating CCN concentrations. All methods demonstrate a strong positive correlation with the observations (Pearson $R > 0.80$) and the NRSME remains in most cases below 1.0 (see Table 2 and Fig. 5). On average over the different supersaturations, the highest correlations and lowest NRMSE are obtained with κ_{opt}, followed by $\kappa_{0.18}$and κ_{bulk}.

https://doi.org/10.5194/egusphere-2025-1602
Preprint. Discussion started: 8 May 2025

The performance skill (i.e. the combination of R and NRMSE, see Fig. 5) depends on the supersaturation. As discussed above, the lowest R and the highest NRMSE occur at the lowest and highest supersaturations i.e., at SS = 0.1% and SS = 1% (see also Table 2). At 0.5% SS, the NRMSE for κ_{bulk} is around 0.49 and the GMB is around 1.38 (see Fig. S11 and Table S2), which is slightly higher than the GMB (1.32) reported by Schmale et al. (2017) for a shorter dataset and a different time period. The best performance skill is obtained at SS = 0.3%, followed closely by SS = 0.2% (see table 2), where predominantly accumulation mode particles activate (see Fig. 3). Given that the typical SS_{max} in stratocumulus clouds in the region are often below 1 % (Roberts et al., 2006; Hegg et al., 2009), the performance at these levels is particularly relevant. Two explanations could account for the large bias at low and high supersaturations: 1) The high flow rate in the CCN counter may hinder smaller particles from growing sufficiently to be detected by the CPC at low supersaturation (see also Ervens et al., 2007 and Lance et al., 2006); 2) It is possible that the assigned hygroscopicity of Aitken mode particles is still higher than it should be (especially at high supersaturations) – e.g., due to too high assumed organic hygroscopicity (see e.g., Rastak et al., 2017).

The results presented in Fig. 4 reveal a systematic overprediction of N_{CCN}. As discussed above, some of this overprediction could be remedied by assuming a size-dependent chemical composition with an enrichment of organics in the Aitken mode – given the expected lower hygroscopicity of the organic as compared with the inorganic aerosol components. Furthermore, previous studies have observed that the hygroscopicity of OA can be lower than 0.1 (see e.g., Rastak et al., 2017 and references therein), thus, an alternative way to optimize the results could be through assuming a size-independent composition but lower organic hygroscopicity. As a conservative test of this approach, we conducted a test assuming organics to be non-hygroscopic, similar to black carbon. In Table 2 and Fig. 5 these calculations are denoted with $\kappa_{org} = 0$. The resulting NRMSE and GMB (see also Fig. S11) suggests that organics in the accumulation mode are likely more hygroscopic, as assuming zero hygroscopicity leads to underprediction of N_{CCN}. Another explanation could be an undetected inorganic component such as sea salt which is not measured by the ACSM. Alternatively, the finding may arise from the initial assumption of the equal distribution of BC among Aitken and accumulation modes. In terms of correlation, κ_{opt} consistently performs better overall (see Table 2), the NRMSE values also being smaller than for the entirely non-hygroscopic organics. This suggests that, compared to the variation in the hygroscopicity parameter of organics with size, that accounting for the size-segregated nature of chemical composition provides a more accurate explanation for the overprediction of CCN than simply non-hygroscopic organics. It is notable, however, that none of the closure methods reproduces the observations, indicating remaining structural model uncertainty or unknown experimental uncertainties.

Table 2. NRMSEs and Pearson's correlation coefficient (R in brackets) corresponding to different methods and supersaturations for all years taken together.

Methods	NRMSE (R) at SS = 0.1%	NRMSE (R) at SS = 0.2%	NRMSE (R) at SS = 0.3%	NRMSE (R) at SS = 0.5%	NRMSE (R) at SS = 1.0%
κ_{bulk}	0.94 (0.78)	0.49 (0.85)	0.49 (0.85)	0.59 (0.84)	0.60 (0.79)
$\kappa_{0.18}$	0.71 (0.74)	0.43 (0.84)	0.42 (0.86)	0.50 (0.85)	0.52 (0.81)
κ_{opt}	0.92 (0.78)	0.46 (0.86)	0.43 (0.87)	0.47 (0.88)	0.44 (0.86)

https://doi.org/10.5194/egusphere-2025-1602
Preprint. Discussion started: 8 May 2025

$\kappa_{org} = 0$	0.62 (0.70)	0.49 (0.75)	0.48 (0.77)	0.46 (0.80)	0.47 (0.77)

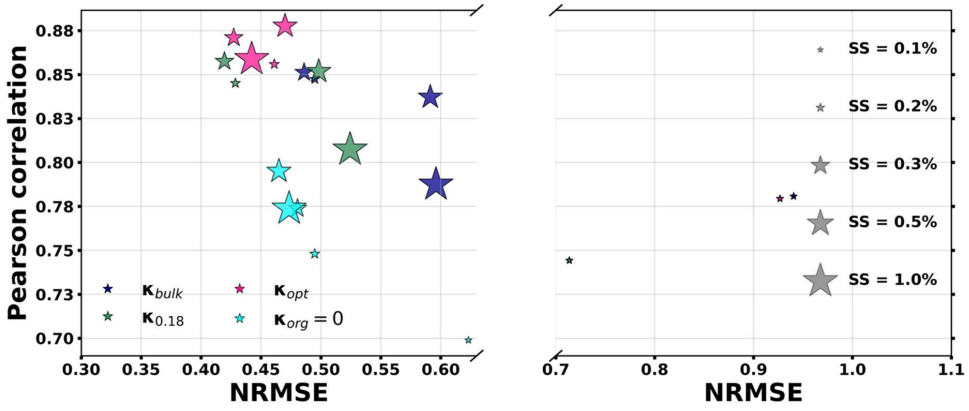

Figure 5: Normalized Root Mean Square Error (NRMSE) and Pearson correlation for different supersaturation (*SS*) levels for all years taken together, comparing four methodologies: κ_{bulk} , $\kappa_{0.18}$, and κ_{opt}, κ_{org}= 0. The two panels split the NRMSE axis to highlight the data in separate ranges, with the left panel covering NRMSE values from 0.3 to 0.6 and the right panel from 0.7 to 1.1. Each point is sized according to the corresponding SS level (0.1%, 0.2%, 0.3%, 0.5%, and 1.0%). The markers are color-coded based on the method for calculating the hygroscopicity parameter, with lines added to represent a discontinuity in the x-axis.

3.3 Insights on size-dependent submicron aerosol composition from inverse CCN closure

The mean of optimized compositions for Aitken and accumulation modes are shown in Fig. 6 (see Table S3 and S4 for medians) in comparison with the bulk composition from the ACSM, with corresponding differences in hygroscopicity shown in Fig. 7. Our findings suggest, in line with previous studies from SMEAR II (e.g., Allan et al., 2006), that the accumulation mode contains a higher mass fraction of inorganic components, resulting in greater hygroscopicity compared to the Aitken mode. Such a difference has also been observed in other similar environments (Timonen et al., 2008; Hao et al., 2013; Levin et al., 2014) as well as in urban Beijing (see also Wu et al., 2016). This disparity in mass fractions of inorganics between the two modes is most pronounced in winter (the relative enrichment in Aitken vs. accumulation model mass fraction being ~156 %) and autumn (the relative enrichment of ~106 %), i.e. the periods when the distinction between Aitken and accumulation modes is most evident (see Fig. 3). This seasonal variation reflects shifts in aerosol sources and processes, and the results are generally in line with what is known. During summer, biogenic SOA is a major source of particulate matter in Hyytiälä (Heikkinen et al., 2021; Yli-Juuti et al., 2022). In contrast, autumn and winter are characterized by a higher mass fraction (and concentration) of inorganic aerosol chemical components (Heikkinen et al., 2020), which highlights the prevalence of transported (Riuttanen et al. 2013) and cloud-processed particles (Isokääntä et al., 2022). Cloud processing leads to both the observed bimodal PNSD (Fig. 3) and a higher sulfate abundance in the accumulation mode (e.g., Leitach et al., 1996; Roelofs et al., 1998; Kreidenweis et al., 2003; Wonaschuetz et al., 2012; Ervens et al., 2018). The difference in relative contribution of chemical species between the Aitken and

https://doi.org/10.5194/egusphere-2025-1602
Preprint. Discussion started: 8 May 2025

accumulation modes also leads to different hygroscopicity (Fig. 7). The density distribution of Aitken and accumulation mode hygroscopicity indicates that the Aitken mode is predominantly organic, with most values clustering around 0.1, while the accumulation mode shows a broader distribution, peaking at nearly twice that value or higher. This significant difference in hygroscopicity between the two modes exceeds the typical variability in hygroscopicity values observed for various soluble chemical components, highlighting distinct chemical compositions and water uptake properties of the two modes i.e. the median hygroscopicity parameter κ_{opt} is ~ 0.11 in the Aitken mode and 0.22-0.29 in the accumulation mode. Overall, the variability between seasons is larger for the accumulation mode (see Fig. 7). The peak in κ occurs in the spring despite the larger contribution of organics to the overall mass. This is explained by the low abundance of eBC in this season. These results are generally in line with previous studies reporting differences in the hygroscopicity of Aitken and accumulation mode-sized particles (Hämeri et al., 2001; Paramonov et al., 2015). Although the seasonal differences in κ_{opt} are not pronounced (median Aitken κ is 0.12 in summer and 0.11 in winter), the Aitken mode has its lowest κ values during autumn and winter, whereas spring and summer display more frequent occurrences of κ values exceeding 0.1 (see Fig. 7), leading to the highest observed values. This seasonal variability coincides with the onset of photochemical reactions during summer, which significantly contribute to the formation of Aitken particles through organic vapor condensation. During the sunlit months, the organic aerosol undergoes photochemical aging, leading to a higher oxygen-to-carbon ratio of the aerosol (Heikkinen et al., 2021), and potentially an increased organic aerosol hygroscopicity (Jimenez et al., 2009).

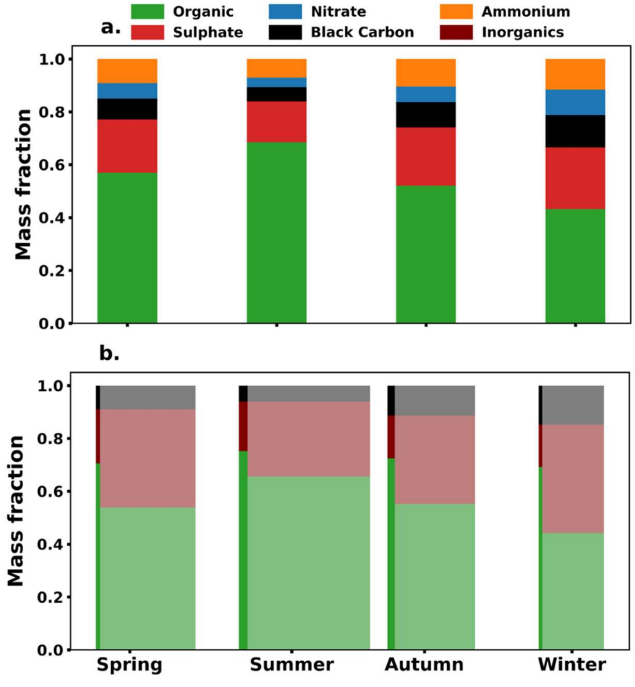

Figure 6: (a) Seasonal mean mass fractions of organic, sulfate, nitrate, black carbon, and ammonia observed by the ACSM and aethalometer. (b) Seasonal optimized mean mass fractions of Aitken and Accumulation modes plotted against different seasons. The stacked bars represent the contributions of organic (green), ammonium sulfate (maroon),

https://doi.org/10.5194/egusphere-2025-1602
Preprint. Discussion started: 8 May 2025

and black carbon (black) components within each mode. Aitken mode is depicted with solid colors, while Accumulation mode is represented with slightly faded colors. The width of the bars has been scaled to the mass concentration in the corresponding mode.

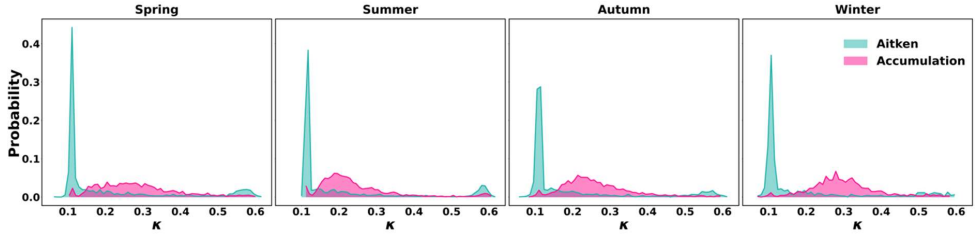

Figure 7: Seasonal distribution of hygroscopicity parameter (κ) for Aitken and accumulation modes. Each panel represents the probabilities of κ values for a specific season: spring, summer, autumn, and winter. The histograms are plotted for the Aitken mode (turquoise) and the accumulation mode (deep pink).

Overall, the median contribution from Aitken mode to the N_{CCN} is < 1 % for 0.1 % *SS*, 3 % for 0.2 % *SS*, 6 % for 0.3 % *SS*, 15 % for 0.5 % *SS*, and 32 % for 1.0 % *SS* – being however highly variable for the whole duration of the time series.

4 Conclusions

In this study, we integrated long-term chemical composition measurements from an Aerosol Chemical Speciation Monitor (ACSM) with Cloud Condensation Nuclei (CCN) observations and aerosol number size distributions. This resulted in ~6,200 concurrent two-hour resolution data points. We used this dataset to evaluate three methods for predicting CCN concentrations based on κ-Köhler theory across varying supersaturations, beginning with two forward closure approaches. The first, a 'bottom-up' method, used ACSM and aethalometer data to estimate the bulk hygroscopicity parameter (κ_{bulk}) for predicting CCN concentrations, while the second approach ($\kappa_{0.18}$) assumed a constant κ value of 0.18, as recommended by Sihto et al. (2011), throughout the study period. We observed that the overall median activation dry diameters (D_{act}) ranged from 54 nm (*SS* = 1%) to 224 nm (*SS* = 0.1%) nm across different months, suggesting that Aitken mode particles contribute to the CCN numbers at this location – besides the well-known contribution of the accumulation mode (Pierce et al., 2012 and references therein). Therefore, the possibility of different chemical composition/hygroscopicity between Aitken and accumulation modes (for e.g. Broekhuizen et al., 2006) motivated us to use an inverse closure technique that involved an optimization algorithm (Nelder-Mead in the Python SciPy library) to determine the optimal modal hygroscopicity (κ_{opt}) by minimizing the Normalized Root Mean Square Error (NRMSE) between observed and predicted CCN concentrations.

CCN concentrations at Hyytiälä exhibit clear seasonal variations, peaking in summer and reaching their lowest in winter, reflecting overall particle number trends. Our closure calculations generally agree reasonably well with observed CCN concentrations, with Pearson correlations exceeding 0.8. However, all of the applied methods tend to overpredict CCN concentrations to varying degrees. Among the methods, κ_{opt} performs the best, as expected, especially at higher supersaturations (0.5% and 1.0%), where both accumulation and Aitken mode

https://doi.org/10.5194/egusphere-2025-1602
Preprint. Discussion started: 8 May 2025

particles can activate, highlighting the importance of accounting for the size-dependent nature of aerosol composition for more accurate CCN predictions. At a supersaturation of 0.3%, which is typical average SS_{max} for stratocumulus clouds, the different methods show similar NRMSE (Normalized Root Mean Squared Error) and GMB (Geometric Mean Bias). Overall, the GMB remains well below 1.3 for both κ_{opt} and $\kappa_{0.18}$ across all supersaturations (see Table S1 in supplementary), except at 0.1%. The best agreement is observed at 0.2% and 0.3% supersaturations, where the GMB is around 1.1 for all methods. However, at a supersaturation of 0.1%, the use of size-dependent composition i.e. κ_{opt} doesn't significantly reduce the error. This suggests that the primary source of the error at this supersaturation arises from another factor — most likely, the substantial measurement uncertainty of the CCN counter at low supersaturation, as previously discussed (see Sect. 3.2).

Our study highlights significant differences in aerosol composition and hygroscopicity between the Aitken and accumulation modes. The accumulation mode has a higher mass fraction of inorganics, leading to greater hygroscopicity compared to the Aitken mode. During summer, biogenic SOA dominates the overall sub-micron aerosol composition, while autumn and winter are characterized by higher concentrations of inorganic components due to transported and cloud-processed particles. The Aitken mode has the lowest κ values in winter, while summer features higher Aitken mode hygroscopicity (lowest accumulation mode κ) possibly due to decreasing BC content which was not accounted for in the calculations. The relative difference in the median Aitken and accumulation κ is most pronounced in winter (~162 %), followed by spring (~134 %), autumn (~116 %) and summer (~85 %) reflecting seasonal shifts in aerosol sources and processes. These seasonal variations are consistent with known atmospheric processes, providing confidence in using CCN data to understand mode composition differences. It is notable however that even the optimized composition does not resolve the over-prediction of the CCN concentrations, indicating an additional structural error in the theoretical approach or experimental uncertainties that we did not account for.

The findings in this study are in line with previous research highlighting distinct differences between Aitken and accumulation mode compositions at Hyytiälä and similar environments (Hao et al., 2013). Previous studies have also demonstrated that accounting for size-dependency improves CCN predictions (Meng et al., 2014). Specifically, our results indicate that the accumulation mode is enriched with sulfate, while the Aitken mode is predominantly organic, in agreement with observed size-dependent chemical compositions using an Aerosol Mass Spectrometer (AMS; Allan et al., 2006). This is furthermore consistent with Mohr et al. (2019), who found that organic vapors significantly contribute to particle growth in the Aitken mode.

The AMS is well-suited for measuring the size-dependent composition of aerosol particles but is less effective for Aitken particles due to their relatively small size and low mass. Similarly, ACSM is biased towards larger particles. In contrast, a CCN counter can measure the growth of small particles to CCN size at high supersaturations, including Aitken particles. Given that the particle growth to CCN size depends on both size and chemistry, observed CCN concentrations are a valuable tool for inversely estimating the chemical composition of Aitken particles. Our study uses this approach, leveraging routine monitoring instruments to estimate size-dependent composition; with the inverse closure method it takes only a few seconds to determine the composition of Aitken and accumulation mode particles for a given time. It should be noted, however, that uncertainties in CCN observations impact the results, as accurate CCN measurements are crucial for size-dependent composition estimates. Moreover, the aerosol particle size distribution should remain relatively stable during a CCN measurement cycle, as the accuracy of predicting CCN spectra is more sensitive to variations in size distribution

https://doi.org/10.5194/egusphere-2025-1602
Preprint. Discussion started: 8 May 2025

than to changes in chemical composition (see e.g. Lowe et al., 2016). In the future, the method applied here should be tested at other locations with varying aerosol chemical compositions. Furthermore, the approach for optimizing the closure (which still left room for improvement) using size-resolved composition should be compared and contrasted with other approaches, e.g. accounting for potential structural issues with the kappa-Köhler model such as the treatment of the surface tension or volatility of the particle components (see e.g. Lowe et al., 2019; Heikkinen et al., 2024).

Data availability. CCN, size distribution and chemical composition data used to generate most of the figures are available at https://github.com/rahulranjanaces/Inverse-closure.git. The raw size distribution data can be accessed at https://smear.avaa.csc.fi/download. The raw CCN and chemical composition data are currently available upon request from the corresponding authors and will be made publicly accessible with a DOI upon final publication.

Code availability. The codes to perform inverse-closure and to generate most of the figures are available at https://github.com/rahulranjanaces/Inverse-closure.git.

Author contribution. RR, IR, LH, DGP and AMLE conceptualized and designed the study. RR implemented the inverse-closure method with initial reference from inverse-modelling setup and guidance by DGP, and performed the majority of the calculations, and the data visualizations. LH conducted the ACSM measurements data and provided the organo-nitrate mass fraction data, while LH and TP jointly analyzed and prepared the ACSM measurement data. AMLE and DGP actively participated in discussion meetings, providing continuous feedback on the results. LRA and PA conducted the CCN and aerosol size distribution measurements and were responsible for the calibrations. KL carried out the eBC observations, processed the data, and provided the final dataset. PB helped with initial setup and implementation of interpolation in calculation of CCN spectra. RR wrote the majority of the manuscript, with IR, LH, AMLE, DGP and KL contributing significantly to the writing and revision process. All co-authors provided their feedback/comments on the manuscript. IR supervised all steps in the process.

Competing interests. One of the authors, Tuukka Petäjä a member of the editorial board for *Atmospheric Chemistry and Physics*. The authors declare no other conflicts of interest.

Acknowledgements. We would like to thank Megan Haslum (Previously at University of Exeter) for her invaluable assistance in set-up of inverse-closure method. We are also thankful to Theodore Khadir for providing us the python implementation of the size distribution fitting algorithm. There has been use of AI tools like Grammerly (https://app.grammarly.com/) and chatGPT (https://chatgpt.com/) to improve the English grammar of a few sentences.

Financial support. This work was supported by the European Union's Horizon 2020 research and innovation programme through the project FORCeS (grant agreement No. 821205) and the INTEGRATE project, funded by the European Research Council Consolidator Grant (No. 865799). Göran Gustafsson foundation is also gratefully acknowledged for financial support. Daniel G. Partridge has received support from NERC (grant

no. NE/W001713/1). Additional support for the SMEAR II station was provided by the University of Helsinki through ACTRIS-HY.

References

Aalto, P., Hämeri, K., Becker, E.D.O., Weber, R., Salm, J., Mäkelä, J., Hoell, C., O'Dowd, C., Karlsson, H., Hansson, H.-C., Väkevä, M., Koponen, I.K., Buzorius, G., Kulmala, M., 2001. Physical characterization of aerosol particles during nucleation events. Tellus, Series B: Chemical and Physical Meteorology 53, 344–358. https://doi.org/10.1034/j.1600-0889.2001.530403.x

Abdul-Razzak, H., Ghan, S.J., 2000. A parameterization of aerosol activation: 2. Multiple aerosol types. Journal of Geophysical Research: Atmospheres 105, 6837–6844. https://doi.org/10.1029/1999JD901161

Abdul-Razzak, H., Ghan, S.J., 2002. A parameterization of aerosol activation 3. Sectional representation. Journal of Geophysical Research: Atmospheres 107, AAC 1-1-AAC 1-6. https://doi.org/10.1029/2001JD000483

Albrecht, B.A., 1989. Aerosols, Cloud Microphysics, and Fractional Cloudiness. Science 245, 1227–1230. https://doi.org/10.1126/science.245.4923.1227

Allan, J.D., Alfarra, M.R., Bower, K.N., Coe, H., Jayne, J.T., Worsnop, D.R., Aalto, P.P., Kulmala, M., Hyötyläinen, T., Cavalli, F., Laaksonen, A., 2006. Size and composition measurements of background aerosol and new particle growth in a Finnish forest during QUEST 2 using an Aerodyne Aerosol Mass Spectrometer. Atmospheric Chemistry and Physics 6, 315–327. https://doi.org/10.5194/acp-6-315-2006

Almeida, G.P., Brito, J., Morales, C.A., Andrade, M.F., Artaxo, P., 2014. Measured and modelled cloud condensation nuclei (CCN) concentration in São Paulo, Brazil: the importance of aerosol size-resolved chemical composition on CCN concentration prediction. Atmospheric Chemistry and Physics 14, 7559–7572. https://doi.org/10.5194/acp-14-7559-2014

Anttila, T., Brus, D., Jaatinen, A., Hyvärinen, A.-P., Kivekäs, N., Romakkaniemi, S., Komppula, M., Lihavainen, H., 2012. Relationships between particles, cloud condensation nuclei and cloud droplet activation during the third Pallas Cloud Experiment. Atmospheric Chemistry and Physics 12, 11435–11450. https://doi.org/10.5194/acp-12-11435-2012

Barahona, D., West, R.E.L., Stier, P., Romakkaniemi, S., Kokkola, H., Nenes, A., 2010. Comprehensively accounting for the effect of giant CCN in cloud activation parameterizations. Atmospheric Chemistry and Physics 10, 2467–2473. https://doi.org/10.5194/acp-10-2467-2010

Bigg, E.K., 1986. Discrepancy between observation and prediction of concentrations of cloud condensation nuclei. Atmospheric Research 20, 81–86. https://doi.org/10.1016/0169-8095(86)90010-4

Blichner, S.M., Yli-Juuti, T., Mielonen, T., Pöhlker, C., Holopainen, E., Heikkinen, L., Mohr, C., Artaxo, P., Carbone, S., Meller, B.B., Quaresma Dias-Júnior, C., Kulmala, M., Petäjä, T., Scott, C.E., Svenhag, C., Nieradzik, L., Sporre, M., Partridge, D.G., Tovazzi, E., Virtanen, A., Kokkola, H., Riipinen, I., 2024. Process-evaluation of forest aerosol-cloud-climate feedback shows clear evidence from observations and large uncertainty in models. Nat Commun 15, 969. https://doi.org/10.1038/s41467-024-45001-y

Bougiatioti, A., Fountoukis, C., Kalivitis, N., Pandis, S.N., Nenes, A., Mihalopoulos, N., 2009. Cloud condensation nuclei measurements in the marine boundary layer of the Eastern Mediterranean: CCN closure

https://doi.org/10.5194/egusphere-2025-1602
Preprint. Discussion started: 8 May 2025

and droplet growth kinetics. Atmospheric Chemistry and Physics 9, 7053–7066. https://doi.org/10.5194/acp-9-7053-2009

Broekhuizen, K., Chang, R.Y.-W., Leaitch, W.R., Li, S.-M., Abbatt, J.P.D., 2006. Closure between measured and modeled cloud condensation nuclei (CCN) using size-resolved aerosol compositions in downtown Toronto. Atmospheric Chemistry and Physics 6, 2513–2524. https://doi.org/10.5194/acp-6-2513-2006

Bulatovic, I., Igel, A.L., Leck, C., Heintzenberg, J., Riipinen, I., Ekman, A.M.L., 2021. The importance of Aitken mode aerosol particles for cloud sustenance in the summertime high Arctic – a simulation study supported by observational data. Atmospheric Chemistry and Physics 21, 3871–3897. https://doi.org/10.5194/acp-21-3871-2021

Cai, M., Tan, H., Chan, C.K., Qin, Y., Xu, H., Li, F., Schurman, M.I., Liu, L., Zhao, J., 2018. The size-resolved cloud condensation nuclei (CCN) activity and its prediction based on aerosol hygroscopicity and composition in the Pearl Delta River (PRD) region during wintertime 2014. Atmospheric Chemistry and Physics 18, 16419–16437. https://doi.org/10.5194/acp-18-16419-2018

Cerully, K.M., Raatikainen, T., Lance, S., Tkacik, D., Tiitta, P., Petäjä, T., Ehn, M., Kulmala, M., Worsnop, D.R., Laaksonen, A., Smith, J.N., Nenes, A., 2011. Aerosol hygroscopicity and CCN activation kinetics in a boreal forest environment during the 2007 EUCAARI campaign. Atmospheric Chemistry and Physics 11, 12369–12386. https://doi.org/10.5194/acp-11-12369-2011

Chuang, P.Y., Collins, D.R., Pawlowska, H., Snider, J.R., Jonsson, H.H., Brenguier, J.L., Flagan, R.C., Seinfeld, J.H., 2000. CCN measurements during ACE-2 and their relationship to cloud microphysical properties. Tellus B 52, 843–867. https://doi.org/10.1034/j.1600-0889.2000.00018.x

Clegg, S.L., Seinfeld, J.H., Brimblecombe, P., 2001. Thermodynamic modelling of aqueous aerosols containing electrolytes and dissolved organic compounds. Journal of Aerosol Science 32, 713–738. https://doi.org/10.1016/S0021-8502(00)00105-1

Croft, B., Martin, R.V., Leaitch, W.R., Burkart, J., Chang, R.Y.-W., Collins, D.B., Hayes, P.L., Hodshire, A.L., Huang, L., Kodros, J.K., Moravek, A., Mungall, E.L., Murphy, J.G., Sharma, S., Tremblay, S., Wentworth, G.R., Willis, M.D., Abbatt, J.P.D., Pierce, J.R., 2019. Arctic marine secondary organic aerosol contributes significantly to summertime particle size distributions in the Canadian Arctic Archipelago. Atmospheric Chemistry and Physics 19, 2787–2812. https://doi.org/10.5194/acp-19-2787-2019

Cubison, M.J., Ervens, B., Feingold, G., Docherty, K.S., Ulbrich, I.M., Shields, L., Prather, K., Hering, S., Jimenez, J.L., 2008. The influence of chemical composition and mixing state of Los Angeles urban aerosol on CCN number and cloud properties. Atmospheric Chemistry and Physics 8, 5649–5667. https://doi.org/10.5194/acp-8-5649-2008

Dada, L., Paasonen, P., Nieminen, T., Buenrostro Mazon, S., Kontkanen, J., Peräkylä, O., Lehtipalo, K., Hussein, T., Petäjä, T., Kerminen, V.-M., Bäck, J., Kulmala, M., 2017. Long-term analysis of clear-sky new particle formation events and nonevents in Hyytiälä. Atmospheric Chemistry and Physics 17, 6227–6241. https://doi.org/10.5194/acp-17-6227-2017

Dal Maso, M., Kulmala, M., Riipinen, I., Wagner, R., Hussein, T., Aalto, P.P., Lehtinen, K.E.J., 2005. Formation and growth of fresh atmospheric aerosols: eight years of aerosol size distribution data from SMEAR II, Hyytiälä, Finland. Boreal Environment Research 10, 323–336.

https://doi.org/10.5194/egusphere-2025-1602
Preprint. Discussion started: 8 May 2025

Ditto, J.C., Barnes, E.B., Khare, P., Takeuchi, M., Joo, T., Bui, A.A.T., Lee-Taylor, J., Eris, G., Chen, Y., Aumont, B., Jimenez, J.L., Ng, N.L., Griffin, R.J., Gentner, D.R., 2018. An omnipresent diversity and variability in the chemical composition of atmospheric functionalized organic aerosol. Commun Chem 1, 1–13. https://doi.org/10.1038/s42004-018-0074-3

Drinovec, L., Močnik, G., Zotter, P., Prévôt, A.S.H., Ruckstuhl, C., Coz, E., Rupakheti, M., Sciare, J., Müller, T., Wiedensohler, A., Hansen, A.D.A., 2015. The "dual-spot" Aethalometer: an improved measurement of aerosol black carbon with real-time loading compensation. Atmospheric Measurement Techniques 8, 1965–1979. https://doi.org/10.5194/amt-8-1965-2015

Duplessis, P., Karlsson, L., Baccarini, A., Wheeler, M., Leaitch, W.R., Svenningsson, B., Leck, C., Schmale, J., Zieger, P., Chang, R.Y.-W., 2024. Highly Hygroscopic Aerosols Facilitate Summer and Early-Autumn Cloud Formation at Extremely Low Concentrations Over the Central Arctic Ocean. Journal of Geophysical Research: Atmospheres 129, e2023JD039159. https://doi.org/10.1029/2023JD039159

El Haber, M., Gérard, V., Kleinheins, J., Ferronato, C., Nozière, B., 2024. Measuring the Surface Tension of Atmospheric Particles and Relevant Mixtures to Better Understand Key Atmospheric Processes. Chem. Rev. 124, 10924–10963. https://doi.org/10.1021/acs.chemrev.4c00173

Ervens, B., Sorooshian, A., Aldhaif, A.M., Shingler, T., Crosbie, E., Ziemba, L., Campuzano-Jost, P., Jimenez, J.L., Wisthaler, A., 2018. Is there an aerosol signature of chemical cloud processing? Atmospheric Chemistry and Physics 18, 16099–16119. https://doi.org/10.5194/acp-18-16099-2018

Ervens, B., Cubison, M.J., Andrews, E., Feingold, G., Ogren, J.A., Jimenez, J.L., Quinn, P.K., Bates, T.S., Wang, J., Zhang, Q., Coe, H., Flynn, M., Allan, J.D., 2010. CCN predictions using simplified assumptions of organic aerosol composition and mixing state: a synthesis from six different locations. Atmospheric Chemistry and Physics 10, 4795–4807. https://doi.org/10.5194/acp-10-4795-2010

Feijó Barreira, L.M., Duporté, G., Rönkkö, T., Parshintsev, J., Hartonen, K., Hyrsky, L., Heikkinen, E., Jussila, M., Kulmala, M., Riekkola, M.-L., 2018. Field measurements of biogenic volatile organic compounds in the atmosphere using solid-phase microextraction Arrow. Atmospheric Measurement Techniques 11, 881–893. https://doi.org/10.5194/amt-11-881-2018

Farmer, D.K., Cappa, C.D., Kreidenweis, S.M., 2015. Atmospheric Processes and Their Controlling Influence on Cloud Condensation Nuclei Activity. Chem. Rev. 115, 4199–4217. https://doi.org/10.1021/cr5006292

Fountoukis, C., Nenes, A., 2005. Continued development of a cloud droplet formation parameterization for global climate models. Journal of Geophysical Research: Atmospheres 110. https://doi.org/10.1029/2004JD005591

Furutani, H., Dall'osto, M., Roberts, G.C., Prather, K.A., 2008. Assessment of the relative importance of atmospheric aging on CCN activity derived from field observations. Atmospheric Environment 42, 3130–3142. https://doi.org/10.1016/j.atmosenv.2007.09.024

Gao, F., Han, L., 2012. Implementing the Nelder-Mead simplex algorithm with adaptive parameters. Comput Optim Appl 51, 259–277. https://doi.org/10.1007/s10589-010-9329-3

Gasparini, R., Li, R., Collins, D.R., Ferrare, R.A., Brackett, V.G., 2006. Application of aerosol hygroscopicity measured at the Atmospheric Radiation Measurement Program's Southern Great Plains site to examine composition and evolution. Journal of Geophysical Research: Atmospheres 111. https://doi.org/10.1029/2004JD005448

https://doi.org/10.5194/egusphere-2025-1602
Preprint. Discussion started: 8 May 2025

842 Ghan, S.J., Abdul-Razzak, H., Nenes, A., Ming, Y., Liu, X., Ovchinnikov, M., Shipway, B., Meskhidze, N., Xu,
843 J., Shi, X., 2011. Droplet nucleation: Physically-based parameterizations and comparative evaluation.
844 Journal of Advances in Modeling Earth Systems 3. https://doi.org/10.1029/2011MS000074
845 Gong, X., Wang, Y., Xie, H., Zhang, J., Lu, Z., Wood, R., Stratmann, F., Wex, H., Liu, X., Wang, J., 2023.
846 Maximum Supersaturation in the Marine Boundary Layer Clouds Over the North Atlantic. AGU Advances
847 4. https://doi.org/10.1029/2022AV000855
848 Guenther, A., Hewitt, C.N., Erickson, D., Fall, R., Geron, C., Graedel, T., Harley, P., Klinger, L., Lerdau, M.,
849 Mckay, W.A., Pierce, T., Scholes, B., Steinbrecher, R., Tallamraju, R., Taylor, J., Zimmerman, P., 1995. A
850 global model of natural volatile organic compound emissions. Journal of Geophysical Research:
851 Atmospheres 100, 8873–8892. https://doi.org/10.1029/94JD02950
852 Gutiérrez, M.S., Furtado, K., 2024. Steady-State Supersaturation Distributions for Clouds under Turbulent
853 Forcing. https://doi.org/10.1175/JAS-D-23-0155.1
854 Hämeri, K., Väkevä, M., Aalto, P.P., Kulmala, M., Swietlicki, E., Zhou, J., Seidl, W., Becker, E., O'dowd, C.D.,
855 2001. Hygroscopic and CCN properties of aerosol particles in boreal forests. Tellus B 53, 359–379.
856 https://doi.org/10.1034/j.1600-0889.2001.530404.x
857 Hao, L., Garmash, O., Ehn, M., Miettinen, P., Massoli, P., Mikkonen, S., Jokinen, T., Roldin, P., Aalto, P., Yli-
858 Juuti, T., Joutsensaari, J., Petäjä, T., Kulmala, M., Lehtinen, K.E.J., Worsnop, D.R., Virtanen, A., 2018.
859 Combined effects of boundary layer dynamics and atmospheric chemistry on aerosol composition during
860 new particle formation periods. Atmospheric Chemistry and Physics 18, 17705–17716.
861 https://doi.org/10.5194/acp-18-17705-2018
862 Hao, L., Romakkaniemi, S., Kortelainen, A., Jaatinen, A., Portin, H., Miettinen, P., Komppula, M., Leskinen, A.,
863 Virtanen, A., Smith, J.N., Sueper, D., Worsnop, D.R., Lehtinen, K.E.J., Laaksonen, A., 2013. Aerosol
864 Chemical Composition in Cloud Events by High Resolution Time-of-Flight Aerosol Mass Spectrometry.
865 Environ. Sci. Technol. 47, 2645–2653. https://doi.org/10.1021/es302889w
866 Hari, P., Kulmala, M., 2005. Station for Measuring Ecosystem-Atmosphere Relations (SMEAR II). Boreal
867 Environment Research 10, 315–322.
868 Hegg, D.A., Covert, D.S., Jonsson, H.H., Woods, R., 2009. Differentiating natural and anthropogenic cloud
869 condensation nuclei in the California coastal zone. Tellus B: Chemical and Physical Meteorology 61.
870 Heikkinen, L., Äijälä, M., Daellenbach, K.R., Chen, G., Garmash, O., Aliaga, D., Graeffe, F., Räty, M., Luoma,
871 K., Aalto, P., Kulmala, M., Petäjä, T., Worsnop, D., Ehn, M., 2021. Eight years of sub-micrometre organic
872 aerosol composition data from the boreal forest characterized using a machine-learning approach.
873 Atmospheric Chemistry and Physics 21, 10081–10109. https://doi.org/10.5194/acp-21-10081-2021
874 Heikkinen, L., Äijälä, M., Riva, M., Luoma, K., Dällenbach, K., Aalto, J., Aalto, P., Aliaga, D., Aurela, M.,
875 Keskinen, H., Makkonen, U., Rantala, P., Kulmala, M., Petäjä, T., Worsnop, D., Ehn, M., 2020. Long-term
876 sub-micrometer aerosol chemical composition in the boreal forest: inter- and intra-annual variability.
877 Atmospheric Chemistry and Physics 20, 3151–3180. https://doi.org/10.5194/acp-20-3151-2020
878 Heikkinen, L., Partridge, D.G., Blichner, S., Huang, W., Ranjan, R., Bowen, P., Tovazzi, E., Petäjä, T., Mohr, C.,
879 Riipinen, I., 2024. Cloud response to co-condensation of water and organic vapors over the boreal forest.
880 Atmospheric Chemistry and Physics 24, 5117–5147. https://doi.org/10.5194/acp-24-5117-2024

https://doi.org/10.5194/egusphere-2025-1602
Preprint. Discussion started: 8 May 2025

Hellén, H., Praplan, A.P., Tykkä, T., Ylivinkka, I., Vakkari, V., Bäck, J., Petäjä, T., Kulmala, M., Hakola, H., 2018. Long-term measurements of volatile organic compounds highlight the importance of sesquiterpenes for the atmospheric chemistry of a boreal forest. Atmospheric Chemistry and Physics 18, 13839–13863. https://doi.org/10.5194/acp-18-13839-2018

Hodzic, A., Aumont, B., Knote, C., Lee-Taylor, J., Madronich, S., Tyndall, G., 2014. Volatility dependence of Henry's law constants of condensable organics: Application to estimate depositional loss of secondary organic aerosols. Geophysical Research Letters 41, 4795–4804. https://doi.org/10.1002/2014GL060649

Hong, J., Äijälä, M., Häme, S.A.K., Hao, L., Duplissy, J., Heikkinen, L.M., Nie, W., Mikkilä, J., Kulmala, M., Prisle, N.L., Virtanen, A., Ehn, M., Paasonen, P., Worsnop, D.R., Riipinen, I., Petäjä, T., Kerminen, V.-M., 2017. Estimates of the organic aerosol volatility in a boreal forest using two independent methods. Atmospheric Chemistry and Physics 17, 4387–4399. https://doi.org/10.5194/acp-17-4387-2017

Hong, J., Kim, J., Nieminen, T., Duplissy, J., Ehn, M., Äijälä, M., Hao, L.Q., Nie, W., Sarnela, N., Prisle, N.L., Kulmala, M., Virtanen, A., Petäjä, T., Kerminen, V.-M., 2015. Relating the hygroscopic properties of submicron aerosol to both gas- and particle-phase chemical composition in a boreal forest environment. Atmospheric Chemistry and Physics 15, 11999–12009. https://doi.org/10.5194/acp-15-11999-2015

Hoppel, W.A., Frick, G.M., Larson, R.E., 1986. Effect of nonprecipitating clouds on the aerosol size distribution in the marine boundary layer. Geophysical Research Letters 13, 125–128. https://doi.org/10.1029/GL013i002p00125

Huang, W., Li, H., Sarnela, N., Heikkinen, L., Tham, Y.J., Mikkilä, J., Thomas, S.J., Donahue, N.M., Kulmala, M., Bianchi, F., 2021. Measurement report: Molecular composition and volatility of gaseous organic compounds in a boreal forest – from volatile organic compounds to highly oxygenated organic molecules. Atmospheric Chemistry and Physics 21, 8961–8977. https://doi.org/10.5194/acp-21-8961-2021

Huang, W., Wu, C., Gao, L., Gramlich, Y., Haslett, S.L., Thornton, J., Lopez-Hilfiker, F.D., Lee, B.H., Song, J., Saathoff, H., Shen, X., Ramisetty, R., Tripathi, S.N., Ganguly, D., Jiang, F., Vallon, M., Schobesberger, S., Yli-Juuti, T., Mohr, C., 2024. Variation in chemical composition and volatility of oxygenated organic aerosol in different rural, urban, and mountain environments. Atmospheric Chemistry and Physics 24, 2607–2624. https://doi.org/10.5194/acp-24-2607-2024

Hussein, T., Dal Maso, M., Petäjä, T., Koponen, I.K., Paatero, P., Aalto, P.P., Hämeri, K., Kulmala, M., 2005. Evaluation of an automatic algorithm for fitting the particle number size distributions. Boreal Environment Research 10, 337–355. http://www.borenv.net/BER/pdfs/ber10/ber10-337.pdf

IPCC, 2021: Climate Change 2021: The Physical Science Basis. Contribution of Working Group I to the Sixth Assessment Report of the Intergovernmental Panel on Climate Change [Masson-Delmotte, V., P. Zhai, A. Pirani, S.L. Connors, C. Péan, S. Berger, N. Caud, Y. Chen, L. Goldfarb, M.I. Gomis, M. Huang, K. Leitzell, E. Lonnoy, J.B.R. Matthews, T.K. Maycock, T. Waterfield, O. Yelekçi, R. Yu, and B. Zhou (eds.)]. Cambridge University Press, Cambridge, United Kingdom and New York, NY, USA, In press, doi:10.1017/9781009157896.

Isokääntä, S., Kim, P., Mikkonen, S., Kühn, T., Kokkola, H., Yli-Juuti, T., Heikkinen, L., Luoma, K., Petäjä, T., Kipling, Z., Partridge, D., Virtanen, A., 2022. The effect of clouds and precipitation on the aerosol concentrations and composition in a boreal forest environment. Atmospheric Chemistry and Physics 22, 11823–11843. https://doi.org/10.5194/acp-22-11823-2022

https://doi.org/10.5194/egusphere-2025-1602
Preprint. Discussion started: 8 May 2025

Jimenez, J.L., Canagaratna, M.R., Donahue, N.M., Prevot, A.S.H., Zhang, Q., Kroll, J.H., DeCarlo, P.F., Allan, J.D., Coe, H., Ng, N.L., Aiken, A.C., Docherty, K.S., Ulbrich, I.M., Grieshop, A.P., Robinson, A.L., Duplissy, J., Smith, J.D., Wilson, K.R., Lanz, V.A., Hueglin, C., Sun, Y.L., Tian, J., Laaksonen, A., Raatikainen, T., Rautiainen, J., Vaattovaara, P., Ehn, M., Kulmala, M., Tomlinson, J.M., Collins, D.R., Cubison, M.J., E., Dunlea, J., Huffman, J.A., Onasch, T.B., Alfarra, M.R., Williams, P.I., Bower, K., Kondo, Y., Schneider, J., Drewnick, F., Borrmann, S., Weimer, S., Demerjian, K., Salcedo, D., Cottrell, L., Griffin, R., Takami, A., Miyoshi, T., Hatakeyama, S., Shimono, A., Sun, J.Y., Zhang, Y.M., Dzepina, K., Kimmel, J.R., Sueper, D., Jayne, J.T., Herndon, S.C., Trimborn, A.M., Williams, L.R., Wood, E.C., Middlebrook, A.M., Kolb, C.E., Baltensperger, U., Worsnop, D.R., 2009. Evolution of Organic Aerosols in the Atmosphere. Science 326, 1525–1529. https://doi.org/10.1126/science.1180353

Jurányi, Z., Gysel, M., Weingartner, E., DeCarlo, P.F., Kammermann, L., Baltensperger, U., 2010. Measured and modelled cloud condensation nuclei number concentration at the high alpine site Jungfraujoch. Atmospheric Chemistry and Physics 10, 7891–7906. https://doi.org/10.5194/acp-10-7891-2010

Khadir, T., 2023. theodorekhadir/Particle_Size_Distribution_Log_Fit_Python: Particle_Size_Distribution_Log_Fit_Python v0.1.0 - Initial Release. https://doi.org/10.5281/zenodo.8017043

Köhler, H., 1936. The nucleus in and the growth of hygroscopic droplets. Trans. Faraday Soc. 32, 1152–1161. https://doi.org/10.1039/TF9363201152

Kreidenweis, S.M., Walcek, C.J., Feingold, G., Gong, W., Jacobson, M.Z., Kim, C.-H., Liu, X., Penner, J.E., Nenes, A., Seinfeld, J.H., 2003. Modification of aerosol mass and size distribution due to aqueous-phase SO2 oxidation in clouds: Comparisons of several models. Journal of Geophysical Research: Atmospheres 108. https://doi.org/10.1029/2002JD002697

Kulmala, M.T., 2018. Build a global Earth observatory. Nature 553, 21–23. https://doi.org/10.1038/d41586-017-08967-y

Laaksonen, A., Kulmala, M., O'Dowd, C.D., Joutsensaari, J., Vaattovaara, P., Mikkonen, S., Lehtinen, K.E.J., Sogacheva, L., Dal Maso, M., Aalto, P., Petäjä, T., Sogachev, A., Yoon, Y.J., Lihavainen, H., Nilsson, D., Facchini, M.C., Cavalli, F., Fuzzi, S., Hoffmann, T., Arnold, F., Hanke, M., Sellegri, K., Umann, B., Junkermann, W., Coe, H., Allan, J.D., Alfarra, M.R., Worsnop, D.R., Riekkola, M.-L., Hyötyläinen, T., Viisanen, Y., 2008. The role of VOC oxidation products in continental new particle formation. Atmospheric Chemistry and Physics 8, 2657–2665. https://doi.org/10.5194/acp-8-2657-2008

Lance, S., Nenes, A., Medina, J., Smith, J.N., 2006. Mapping the Operation of the DMT Continuous Flow CCN Counter. Aerosol Science and Technology 40, 242–254. https://doi.org/10.1080/02786820500543290

Leaitch, W.R., 1996. Observations Pertaining to the Effect of Chemical Transformation in Cloud on the Anthropogenic Aerosol Size Distribution. Aerosol Science and Technology 25, 157–173. https://doi.org/10.1080/02786829608965388

Lee, L.A., Carslaw, K.S., Pringle, K.J., Mann, G.W., 2012. Mapping the uncertainty in global CCN using emulation. Atmospheric Chemistry and Physics 12, 9739–9751. https://doi.org/10.5194/acp-12-9739-2012

Lehtipalo, K., Yan, C., Dada, L., Bianchi, F., Xiao, M., Wagner, R., Stolzenburg, D., Ahonen, L.R., Amorim, A., Baccarini, A., Bauer, P.S., Baumgartner, B., Bergen, A., Bernhammer, A.-K., Breitenlechner, M., Brilke, S., Buchholz, A., Mazon, S.B., Chen, D., Chen, X., Dias, A., Dommen, J., Draper, D.C., Duplissy, J., Ehn,

https://doi.org/10.5194/egusphere-2025-1602
Preprint. Discussion started: 8 May 2025

M., Finkenzeller, H., Fischer, L., Frege, C., Fuchs, C., Garmash, O., Gordon, H., Hakala, J., He, X., Heikkinen, L., Heinritzi, M., Helm, J.C., Hofbauer, V., Hoyle, C.R., Jokinen, T., Kangasluoma, J., Kerminen, V.-M., Kim, C., Kirkby, J., Kontkanen, J., Kürten, A., Lawler, M.J., Mai, H., Mathot, S., Mauldin, R.L., Molteni, U., Nichman, L., Nie, W., Nieminen, T., Ojdanic, A., Onnela, A., Passananti, M., Petäjä, T., Piel, F., Pospisilova, V., Quéléver, L.L.J., Rissanen, M.P., Rose, C., Sarnela, N., Schallhart, S., Schuchmann, S., Sengupta, K., Simon, M., Sipilä, M., Tauber, C., Tomé, A., Tröstl, J., Väisänen, O., Vogel, A.L., Volkamer, R., Wagner, A.C., Wang, M., Weitz, L., Wimmer, D., Ye, P., Ylisirniö, A., Zha, Q., Carslaw, K.S., Curtius, J., Donahue, N.M., Flagan, R.C., Hansel, A., Riipinen, I., Virtanen, A., Winkler, P.M., Baltensperger, U., Kulmala, M., Worsnop, D.R., 2018. Multicomponent new particle formation from sulfuric acid, ammonia, and biogenic vapors. Science Advances 4, eaau5363. https://doi.org/10.1126/sciadv.aau5363

Levin, E.J.T., Prenni, A.J., Palm, B.B., Day, D.A., Campuzano-Jost, P., Winkler, P.M., Kreidenweis, S.M., DeMott, P.J., Jimenez, J.L., Smith, J.N., 2014. Size-resolved aerosol composition and its link to hygroscopicity at a forested site in Colorado. Atmospheric Chemistry and Physics 14, 2657–2667. https://doi.org/10.5194/acp-14-2657-2014

Liu, P., Song, M., Zhao, T., Gunthe, S.S., Ham, S., He, Y., Qin, Y.M., Gong, Z., Amorim, J.C., Bertram, A.K., Martin, S.T., 2018. Resolving the mechanisms of hygroscopic growth and cloud condensation nuclei activity for organic particulate matter. Nat Commun 9, 4076. https://doi.org/10.1038/s41467-018-06622-2

Liu, P., Ziemann, P.J., Kittelson, D.B., McMurry, P.H., 1995a. Generating Particle Beams of Controlled Dimensions and Divergence: I. Theory of Particle Motion in Aerodynamic Lenses and Nozzle Expansions. Aerosol Science and Technology 22, 293–313. https://doi.org/10.1080/02786829408959748

Liu, P.S.K., Deng, R., Smith, K.A., Williams, L.R., Jayne, J.T., Canagaratna, M.R., Moore, K., Onasch, T.B., Worsnop, D.R., Deshler, T., 2007. Transmission Efficiency of an Aerodynamic Focusing Lens System: Comparison of Model Calculations and Laboratory Measurements for the Aerodyne Aerosol Mass Spectrometer. Aerosol Science and Technology 41, 721–733. https://doi.org/10.1080/02786820701422278

Liu, P.S.K., Leaitch, W.R., Banic, C.M., Li, S.-M., Ngo, D., Megaw, W.J., 1996. Aerosol observations at Chebogue Point during the 1993 North Atlantic Regional Experiment: Relationships among cloud condensation nuclei, size distribution, and chemistry. Journal of Geophysical Research: Atmospheres 101, 28971–28990. https://doi.org/10.1029/96JD00445

Liu, X., Wang, J., 2010. How important is organic aerosol hygroscopicity to aerosol indirect forcing? Environ. Res. Lett. 5, 044010. https://doi.org/10.1088/1748-9326/5/4/044010

Lowe, S., Partridge, D.G., Topping, D., Stier, P., 2016. Inverse modelling of Köhler theory – Part 1: A response surface analysis of CCN spectra with respect to surface-active organic species. Atmospheric Chemistry and Physics 16, 10941–10963. https://doi.org/10.5194/acp-16-10941-2016

Luoma, K., Niemi, J.V., Aurela, M., Fung, P.L., Helin, A., Hussein, T., Kangas, L., Kousa, A., Rönkkö, T., Timonen, H., Virkkula, A., Petäjä, T., 2021. Spatiotemporal variation and trends in equivalent black carbon in the Helsinki metropolitan area in Finland. Atmospheric Chemistry and Physics 21, 1173–1189. https://doi.org/10.5194/acp-21-1173-2021

https://doi.org/10.5194/egusphere-2025-1602
Preprint. Discussion started: 8 May 2025

999 Mäkelä, J.M., Aalto, P., Jokinen, V., Pohja, T., Nissinen, A., Palmroth, S., Markkanen, T., Seitsonen, K.,
1000 Lihavainen, H., Kulmala, M., 1997a. Observations of ultrafine aerosol particle formation and growth in
1001 boreal forest. Geophysical Research Letters 24, 1219–1222. https://doi.org/10.1029/97GL00920
1002 Mäkelä, J.M., Kulmala, M., Aalto, P., Toivonen, A., Pohja, T., 1997b. Continuous Measurements of Submicron
1003 Particle Size Distribution at Boreal Forest Station in Southern Finland. Journal of Aerosol Science 1001,
1004 S403–S404.
1005 Martin, M., Chang, R.Y.-W., Sierau, B., Sjogren, S., Swietlicki, E., Abbatt, J.P.D., Leck, C., Lohmann, U., 2011.
1006 Cloud condensation nuclei closure study on summer arctic aerosol. Atmospheric Chemistry and Physics 11,
1007 11335–11350. https://doi.org/10.5194/acp-11-11335-2011
1008 McFiggans, G., Artaxo, P., Baltensperger, U., Coe, H., Facchini, M.C., Feingold, G., Fuzzi, S., Gysel, M.,
1009 Laaksonen, A., Lohmann, U., Mentel, T.F., Murphy, D.M., O'Dowd, C.D., Snider, J.R., Weingartner, E.,
1010 2006b. The effect of physical and chemical aerosol properties on warm cloud droplet activation.
1011 Atmospheric Chemistry and Physics 6, 2593–2649. https://doi.org/10.5194/acp-6-2593-2006
1012 Medina, J., Nenes, A., Sotiropoulou, R.-E.P., Cottrell, L.D., Ziemba, L.D., Beckman, P.J., Griffin, R.J., 2007.
1013 Cloud condensation nuclei closure during the International Consortium for Atmospheric Research on
1014 Transport and Transformation 2004 campaign: Effects of size-resolved composition. Journal of Geophysical
1015 Research: Atmospheres 112. https://doi.org/10.1029/2006JD007588
1016 Meng, J.W., Yeung, M.C., Li, Y.J., Lee, B.Y.L., Chan, C.K., 2014. Size-resolved cloud condensation nuclei
1017 (CCN) activity and closure analysis at the HKUST Supersite in Hong Kong. Atmospheric Chemistry and
1018 Physics 14, 10267–10282. https://doi.org/10.5194/acp-14-10267-2014
1019 Merikanto, J., Spracklen, D.V., Mann, G.W., Pickering, S.J., Carslaw, K.S., 2009. Impact of nucleation on global
1020 CCN. Atmospheric Chemistry and Physics 9, 8601–8616. https://doi.org/10.5194/acp-9-8601-2009
1021 Metzger, A., Verheggen, B., Dommen, J., Duplissy, J., Prevot, A.S.H., Weingartner, E., Riipinen, I., Kulmala,
1022 M., Spracklen, D.V., Carslaw, K.S., Baltensperger, U., 2010. Evidence for the role of organics in aerosol
1023 particle formation under atmospheric conditions. Proceedings of the National Academy of Sciences 107,
1024 6646–6651. https://doi.org/10.1073/pnas.0911330107
1025 Mohr, C., Thornton, J.A., Heitto, A., Lopez-Hilfiker, F.D., Lutz, A., Riipinen, I., Hong, J., Donahue, N.M.,
1026 Hallquist, M., Petäjä, T., Kulmala, M., Yli-Juuti, T., 2019. Molecular identification of organic vapors
1027 driving atmospheric nanoparticle growth. Nat Commun 10, 4442. https://doi.org/10.1038/s41467-019-
1028 12473-2
1029 Moore, R.H., Raatikainen, T., Langridge, J.M., Bahreini, R., Brock, C.A., Holloway, J.S., Lack, D.A.,
1030 Middlebrook, A.M., Perring, A.E., Schwarz, J.P., Spackman, J.R., Nenes, A., 2012. CCN Spectra,
1031 Hygroscopicity, and Droplet Activation Kinetics of Secondary Organic Aerosol Resulting from the 2010
1032 Deepwater Horizon Oil Spill. Environ. Sci. Technol. 46, 3093–3100. https://doi.org/10.1021/es203362w
1033 Morales Betancourt, R., Nenes, A., 2014. Droplet activation parameterization: the population-splitting concept
1034 revisited. Geoscientific Model Development 7, 2345–2357. https://doi.org/10.5194/gmd-7-2345-2014
1035 Mulcahy, J.P., Johnson, C., Jones, C.G., Povey, A.C., Scott, C.E., Sellar, A., Turnock, S.T., Woodhouse, M.T.,
1036 Abraham, N.L., Andrews, M.B., Bellouin, N., Browse, J., Carslaw, K.S., Dalvi, M., Folberth, G.A., Glover,
1037 M., Grosvenor, D.P., Hardacre, C., Hill, R., Johnson, B., Jones, A., Kipling, Z., Mann, G., Mollard, J.,
1038 O'Connor, F.M., Palmiéri, J., Reddington, C., Rumbold, S.T., Richardson, M., Schutgens, N.A.J., Stier, P.,

https://doi.org/10.5194/egusphere-2025-1602
Preprint. Discussion started: 8 May 2025

Stringer, M., Tang, Y., Walton, J., Woodward, S., Yool, A., 2020. Description and evaluation of aerosol in UKESM1 and HadGEM3-GC3.1 CMIP6 historical simulations. Geoscientific Model Development 13, 6383–6423. https://doi.org/10.5194/gmd-13-6383-2020

Nenes, A., Pandis, S.N., Pilinis, C., 1999. Continued development and testing of a new thermodynamic aerosol module for urban and regional air quality models. Atmospheric Environment 33, 1553–1560. https://doi.org/10.1016/S1352-2310(98)00352-5

Nenes, A., Pandis, S.N., Pilinis, C., 1998. ISORROPIA: A new thermodynamic equilibrium model for multiphase multicomponent inorganic aerosols. Aquatic Geochemistry 4, 123–152. https://doi.org/10.1023/A:1009604003981

Nenes, A., Seinfeld, J.H., 2003. Parameterization of cloud droplet formation in global climate models. Journal of Geophysical Research: Atmospheres 108. https://doi.org/10.1029/2002JD002911

Ng, N.L., Herndon, S.C., Trimborn, A., Canagaratna, M.R., Croteau, P.L., Onasch, T.B., Sueper, D., Worsnop, D.R., Zhang, Q., Sun, Y.L., Jayne, J.T., 2011. An Aerosol Chemical Speciation Monitor (ACSM) for Routine Monitoring of the Composition and Mass Concentrations of Ambient Aerosol. Aerosol Science and Technology 45, 780–794. https://doi.org/10.1080/02786826.2011.560211

Nieminen, T., Asmi, A., Dal Maso, M., Aalto, P., Keronen, P., Petäjä, T., Kulmala, M., Kerminen, V.-M., 2014b. Trends in atmospheric new-particle formation: 16 years of observations in a boreal-forest environment. BOREAL ENVIRONMENT RESEARCH 19, 191–214. http://www.borenv.net/BER/pdfs/ber19/ber19B-191.pdf

Nozière, B., Kalberer, M., Claeys, M., Allan, J., D'Anna, B., Decesari, S., Finessi, E., Glasius, M., Grgić, I., Hamilton, J.F., Hoffmann, T., Iinuma, Y., Jaoui, M., Kahnt, A., Kampf, C.J., Kourtchev, I., Maenhaut, W., Marsden, N., Saarikoski, S., Schnelle-Kreis, J., Surratt, J.D., Szidat, S., Szmigielski, R., Wisthaler, A., 2015. The Molecular Identification of Organic Compounds in the Atmosphere: State of the Art and Challenges. Chem. Rev. 115, 3919–3983. https://doi.org/10.1021/cr5003485

Paasonen, P., Asmi, A., Petäjä, T., Kajos, M.K., Äijälä, M., Junninen, H., Holst, T., Abbatt, J.P.D., Arneth, A., Birmili, W., van der Gon, H.D., Hamed, A., Hoffer, A., Laakso, L., Laaksonen, A., Richard Leaitch, W., Plass-Dülmer, C., Pryor, S.C., Räisänen, P., Swietlicki, E., Wiedensohler, A., Worsnop, D.R., Kerminen, V.-M., Kulmala, M., 2013. Warming-induced increase in aerosol number concentration likely to moderate climate change. Nature Geosci 6, 438–442. https://doi.org/10.1038/ngeo1800

Paramonov, M., Aalto, P.P., Asmi, A., Prisle, N., Kerminen, V.-M., Kulmala, M., Petäjä, T., 2013. The analysis of size-segregated cloud condensation nuclei counter (CCNC) data and its implications for cloud droplet activation. Atmospheric Chemistry and Physics 13, 10285–10301. https://doi.org/10.5194/acp-13-10285-2013

Paramonov, M., Kerminen, V.-M., Gysel, M., Aalto, P.P., Andreae, M.O., Asmi, E., Baltensperger, U., Bougiatioti, A., Brus, D., Frank, G.P., Good, N., Gunthe, S.S., Hao, L., Irwin, M., Jaatinen, A., Jurányi, Z., King, S.M., Kortelainen, A., Kristensson, A., Lihavainen, H., Kulmala, M., Lohmann, U., Martin, S.T., McFiggans, G., Mihalopoulos, N., Nenes, A., O'Dowd, C.D., Ovadnevaite, J., Petäjä, T., Pöschl, U., Roberts, G.C., Rose, D., Svenningsson, B., Swietlicki, E., Weingartner, E., Whitehead, J., Wiedensohler, A., Wittbom, C., Sierau, B., 2015. A synthesis of cloud condensation nuclei counter (CCNC) measurements

https://doi.org/10.5194/egusphere-2025-1602
Preprint. Discussion started: 8 May 2025

within the EUCAARI network. Atmospheric Chemistry and Physics 15, 12211–12229. https://doi.org/10.5194/acp-15-12211-2015

Partridge, D.G., Vrugt, J.A., Tunved, P., Ekman, A.M.L., Gorea, D., Sorooshian, A., 2011. Inverse modeling of cloud-aerosol interactions – Part 1: Detailed response surface analysis. Atmospheric Chemistry and Physics 11, 7269–7287. https://doi.org/10.5194/acp-11-7269-2011

Partridge, D.G., Vrugt, J.A., Tunved, P., Ekman, A.M.L., Struthers, H., Sorooshian, A., 2012. Inverse modelling of cloud-aerosol interactions – Part 2: Sensitivity tests on liquid phase clouds using a Markov chain Monte Carlo based simulation approach. Atmospheric Chemistry and Physics 12, 2823–2847. https://doi.org/10.5194/acp-12-2823-2012

Patokoski, J., Ruuskanen, T.M., Kajos, M.K., Taipale, R., Rantala, P., Aalto, J., Ryyppö, T., Nieminen, T., Hakola, H., Rinne, J., 2015. Sources of long-lived atmospheric VOCs at the rural boreal forest site, SMEAR II. Atmospheric Chemistry and Physics 15, 13413–13432. https://doi.org/10.5194/acp-15-13413-2015

Petäjä, T., Tabakova, K., Manninen, A., Ezhova, E., O'Connor, E., Moisseev, D., Sinclair, V.A., Backman, J., Levula, J., Luoma, K., Virkkula, A., Paramonov, M., Räty, M., Äijälä, M., Heikkinen, L., Ehn, M., Sipilä, M., Yli-Juuti, T., Virtanen, A., Ritsche, M., Hickmon, N., Pulik, G., Rosenfeld, D., Worsnop, D.R., Bäck, J., Kulmala, M., Kerminen, V.-M., 2022. Influence of biogenic emissions from boreal forests on aerosol–cloud interactions. Nat. Geosci. 15, 42–47. https://doi.org/10.1038/s41561-021-00876-0

Petters, M.D., Kreidenweis, S.M., 2007. A single parameter representation of hygroscopic growth and cloud condensation nucleus activity. Atmospheric Chemistry and Physics 7, 1961–1971. https://doi.org/10.5194/acp-7-1961-2007

Pierce, J.R., Leaitch, W.R., Liggio, J., Westervelt, D.M., Wainwright, C.D., Abbatt, J.P.D., Ahlm, L., Al-Basheer, W., Cziczo, D.J., Hayden, K.L., Lee, A.K.Y., Li, S.-M., Russell, L.M., Sjostedt, S.J., Strawbridge, K.B., Travis, M., Vlasenko, A., Wentzell, J.J.B., Wiebe, H.A., Wong, J.P.S., Macdonald, A.M., 2012. Nucleation and condensational growth to CCN sizes during a sustained pristine biogenic SOA event in a forested mountain valley. Atmospheric Chemistry and Physics 12, 3147–3163. https://doi.org/10.5194/acp-12-3147-2012

Pöhlker, M.L., Pöhlker, C., Quaas, J., Mülmenstädt, J., Pozzer, A., Andreae, M.O., Artaxo, P., Block, K., Coe, H., Ervens, B., Gallimore, P., Gaston, C.J., Gunthe, S.S., Henning, S., Herrmann, H., Krüger, O.O., McFiggans, G., Poulain, L., Raj, S.S., Reyes-Villegas, E., Royer, H.M., Walter, D., Wang, Y., Pöschl, U., 2023. Global organic and inorganic aerosol hygroscopicity and its effect on radiative forcing. Nat Commun 14, 6139. https://doi.org/10.1038/s41467-023-41695-8

Pöhlker, M.L., Zhang, M., Campos Braga, R., Krüger, O.O., Pöschl, U., Ervens, B., 2021. Aitken mode particles as CCN in aerosol- and updraft-sensitive regimes of cloud droplet formation. Atmospheric Chemistry and Physics 21, 11723–11740. https://doi.org/10.5194/acp-21-11723-2021

Prisle, N.L., Raatikainen, T., Laaksonen, A., Bilde, M., 2010. Surfactants in cloud droplet activation: mixed organic-inorganic particles. Atmospheric Chemistry and Physics 10, 5663–5683. https://doi.org/10.5194/acp-10-5663-2010

Pruppacher, H.R., Klett, J.D., 2010. Microphysics of Clouds and Precipitation, Atmospheric and Oceanographic Sciences Library. Springer Netherlands, Dordrecht. https://doi.org/10.1007/978-0-306-48100-0

https://doi.org/10.5194/egusphere-2025-1602
Preprint. Discussion started: 8 May 2025

Qiao, X., Yan, C., Li, X., Guo, Y., Yin, R., Deng, C., Li, C., Nie, W., Wang, M., Cai, R., Huang, D., Wang, Z., Yao, L., Worsnop, D.R., Bianchi, F., Liu, Y., Donahue, N.M., Kulmala, M., Jiang, J., 2021. Contribution of Atmospheric Oxygenated Organic Compounds to Particle Growth in an Urban Environment. Environ. Sci. Technol. 55, 13646–13656. https://doi.org/10.1021/acs.est.1c02095

Quinn, P.K., Bates, T.S., Coffman, D.J., Covert, D.S., 2008. Influence of particle size and chemistry on the cloud nucleating properties of aerosols. Atmospheric Chemistry and Physics 8, 1029–1042. https://doi.org/10.5194/acp-8-1029-2008

Raga, G.B., Jonas, P.R., 1995. Vertical distribution of aerosol particles and CCN in clear air around the British Isles. Atmospheric Environment 29, 673–684. https://doi.org/10.1016/1352-2310(94)00314-B

Rejano, F., Casans, A., Via, M., Casquero-Vera, J.A., Castillo, S., Lyamani, H., Cazorla, A., Andrews, E., Pérez-Ramírez, D., Alastuey, A., Gómez-Moreno, F.J., Alados-Arboledas, L., Olmo, F.J., Titos, G., 2024. CCN estimations at a high-altitude remote site: role of organic aerosol variability and hygroscopicity. EGUsphere 1–39. https://doi.org/10.5194/egusphere-2024-1059

Reutter, P., Su, H., Trentmann, J., Simmel, M., Rose, D., Gunthe, S.S., Wernli, H., Andreae, M.O., Pöschl, U., 2009. Aerosol- and updraft-limited regimes of cloud droplet formation: influence of particle number, size and hygroscopicity on the activation of cloud condensation nuclei (CCN). Atmospheric Chemistry and Physics 9, 7067–7080. https://doi.org/10.5194/acp-9-7067-2009

Riipinen, I., Pierce, J.R., Yli-Juuti, T., Nieminen, T., Häkkinen, S., Ehn, M., Junninen, H., Lehtipalo, K., Petäjä, T., Slowik, J., Chang, R., Shantz, N.C., Abbatt, J., Leaitch, W.R., Kerminen, V.-M., Worsnop, D.R., Pandis, S.N., Donahue, N.M., Kulmala, M., 2011. Organic condensation: a vital link connecting aerosol formation to cloud condensation nuclei (CCN) concentrations. Atmospheric Chemistry and Physics 11, 3865–3878. https://doi.org/10.5194/acp-11-3865-2011

Riipinen, I., Rastak, N., Pandis, S.N., 2015. Connecting the solubility and CCN activation of complex organic aerosols: a theoretical study using solubility distributions. Atmospheric Chemistry and Physics 15, 6305–6322. https://doi.org/10.5194/acp-15-6305-2015

Rissman, T.A., VanReken, T.M., Wang, J., Gasparini, R., Collins, D.R., Jonsson, H.H., Brechtel, F.J., Flagan, R.C., Seinfeld, J.H., 2006. Characterization of ambient aerosol from measurements of cloud condensation nuclei during the 2003 Atmospheric Radiation Measurement Aerosol Intensive Observational Period at the Southern Great Plains site in Oklahoma. Journal of Geophysical Research: Atmospheres 111. https://doi.org/10.1029/2004JD005695

Riuttanen, L., Hulkkonen, M., Dal Maso, M., Junninen, H., Kulmala, M., 2013. Trajectory analysis of atmospheric transport of fine particles, SO_2, NO_x and O_3 to the SMEAR II station in Finland in 1996–2008. Atmospheric Chemistry and Physics 13, 2153–2164. https://doi.org/10.5194/acp-13-2153-2013

Roberts, G., Mauger, G., Hadley, O., Ramanathan, V., 2006. North American and Asian aerosols over the eastern Pacific Ocean and their role in regulating cloud condensation nuclei. Journal of Geophysical Research: Atmospheres 111. https://doi.org/10.1029/2005JD006661

Roberts, G.C., Nenes, A., 2005. A Continuous-Flow Streamwise Thermal-Gradient CCN Chamber for Atmospheric Measurements. Aerosol Science and Technology 39, 206–221. https://doi.org/10.1080/027868290913988

https://doi.org/10.5194/egusphere-2025-1602
Preprint. Discussion started: 8 May 2025

Robinson, A.L., Donahue, N.M., Shrivastava, M.K., Weitkamp, E.A., Sage, A.M., Grieshop, A.P., Lane, T.E., Pierce, J.R., Pandis, S.N., 2007. Rethinking Organic Aerosols: Semivolatile Emissions and Photochemical Aging. Science 315, 1259–1262. https://doi.org/10.1126/science.1133061

Roelofs, G.-J. a N., Lelieveld, J., Ganzeveld, L., 1998. Simulation of global sulfate distribution and the influence on effective cloud drop radii with a coupled photochemistry sulfur cycle model. Tellus B 50, 224–242. https://doi.org/10.1034/j.1600-0889.1998.t01-2-00002.x

Rogers, R.R., Yau, M.K., 1989. A short course in cloud physics / by R.R. Rogers and M.K. Yau., Third edition, International series in natural philosophy; v. 113. Pergamon Press, Oxford [England]; New York.

Rose, D., Gunthe, S.S., Mikhailov, E., Frank, G.P., Dusek, U., Andreae, M.O., Pöschl, U., 2008a. Calibration and measurement uncertainties of a continuous-flow cloud condensation nuclei counter (DMT-CCNC): CCN activation of ammonium sulfate and sodium chloride aerosol particles in theory and experiment. Atmospheric Chemistry and Physics 8, 1153–1179. https://doi.org/10.5194/acp-8-1153-2008

Ruehl, C.R., Chuang, P.Y., Nenes, A., Cappa, C.D., Kolesar, K.R., Goldstein, A.H., 2012. Strong evidence of surface tension reduction in microscopic aqueous droplets. Geophysical Research Letters 39. https://doi.org/10.1029/2012GL053706

Saliba, G., Sanchez, K.J., Russell, L.M., Twohy, C.H., Roberts, G.C., Lewis, S., Dedrick, J., McCluskey, C.S., Moore, K., DeMott, P.J., Toohey, D.W., 2020. Organic composition of three different size ranges of aerosol particles over the Southern Ocean. Aerosol Science and Technology 55, 268–288. https://doi.org/10.1080/02786826.2020.1845296

Schmale, J., Henning, S., Decesari, S., Henzing, B., Keskinen, H., Sellegri, K., Ovadnevaite, J., Pöhlker, M.L., Brito, J., Bougiatioti, A., Kristensson, A., Kalivitis, N., Stavroulas, I., Carbone, S., Jefferson, A., Park, M., Schlag, P., Iwamoto, Y., Aalto, P., Äijälä, M., Bukowiecki, N., Ehn, M., Frank, G., Fröhlich, R., Frumau, A., Herrmann, E., Herrmann, H., Holzinger, R., Kos, G., Kulmala, M., Mihalopoulos, N., Nenes, A., O'Dowd, C., Petäjä, T., Picard, D., Pöhlker, C., Pöschl, U., Poulain, L., Prévôt, A.S.H., Swietlicki, E., Andreae, M.O., Artaxo, P., Wiedensohler, A., Ogren, J., Matsuki, A., Yum, S.S., Stratmann, F., Baltensperger, U., Gysel, M., 2018. Long-term cloud condensation nuclei number concentration, particle number size distribution and chemical composition measurements at regionally representative observatories. Atmospheric Chemistry and Physics 18, 2853–2881. https://doi.org/10.5194/acp-18-2853-2018

Sihto, S.-L., Mikkilä, J., Vanhanen, J., Ehn, M., Liao, L., Lehtipalo, K., Aalto, P.P., Duplissy, J., Petäjä, T., Kerminen, V.-M., Boy, M., Kulmala, M., 2011. Seasonal variation of CCN concentrations and aerosol activation properties in boreal forest. Atmospheric Chemistry and Physics 11, 13269–13285. https://doi.org/10.5194/acp-11-13269-2011

Simpson, E., Connolly, P., McFiggans, G., 2014. An investigation into the performance of four cloud droplet activation parameterisations. Geoscientific Model Development 7, 1535–1542. https://doi.org/10.5194/gmd-7-1535-2014

Spracklen, D.V., Bonn, B., Carslaw, K.S., 2008. Boreal forests, aerosols and the impacts on clouds and climate. Philosophical Transactions of the Royal Society A: Mathematical, Physical and Engineering Sciences 366, 4613–4626. https://doi.org/10.1098/rsta.2008.0201

https://doi.org/10.5194/egusphere-2025-1602
Preprint. Discussion started: 8 May 2025

Stroud, C.A., Nenes, A., Jimenez, J.L., DeCarlo, P.F., Huffman, J.A., Bruintjes, R., Nemitz, E., Delia, A.E., Toohey, D.W., Guenther, A.B., Nandi, S., 2007. Cloud Activating Properties of Aerosol Observed during CELTIC. https://doi.org/10.1175/JAS3843.1

Timonen, H., Saarikoski, S., Tolonen-Kivimäki, O., Aurela, M., Saarnio, K., Petäjä, T., Aalto, P.P., Kulmala, M., Pakkanen, T., Hillamo, R., 2008. Size distributions, sources and source areas of water-soluble organic carbon in urban background air. Atmospheric Chemistry and Physics 8, 5635–5647. https://doi.org/10.5194/acp-8-5635-2008

Twomey, S., 1974. Pollution and the planetary albedo. Atmospheric Environment (1967) 8, 1251–1256. https://doi.org/10.1016/0004-6981(74)90004-3

Tunved, P., Hansson, H.-C., Kerminen, V.-M., Ström, J., Maso, M.D., Lihavainen, H., Viisanen, Y., Aalto, P.P., Komppula, M., Kulmala, M., 2006. High Natural Aerosol Loading over Boreal Forests. Science 312, 261–263. https://doi.org/10.1126/science.1123052

VanReken, T.M., Rissman, T.A., Roberts, G.C., Varutbangkul, V., Jonsson, H.H., Flagan, R.C., Seinfeld, J.H., 2003. Toward aerosol/cloud condensation nuclei (CCN) closure during CRYSTAL-FACE. Journal of Geophysical Research: Atmospheres 108. https://doi.org/10.1029/2003JD003582

Virkkula, A., Mäkelä, T., Hillamo, R., Yli-Tuomi, T., Hirsikko, A., Hämeri, K., Koponen, I.K., 2007. A Simple Procedure for Correcting Loading Effects of Aethalometer Data. Journal of the Air & Waste Management Association 57, 1214–1222. https://doi.org/10.3155/1047-3289.57.10.1214

Williams, J., Crowley, J., Fischer, H., Harder, H., Martinez, M., Petäjä, T., Rinne, J., Bäck, J., Boy, M., Dal Maso, M., Hakala, J., Kajos, M., Keronen, P., Rantala, P., Aalto, J., Aaltonen, H., Paatero, J., Vesala, T., Hakola, H., Levula, J., Pohja, T., Herrmann, F., Auld, J., Mesarchaki, E., Song, W., Yassaa, N., Nölscher, A., Johnson, A.M., Custer, T., Sinha, V., Thieser, J., Pouvesle, N., Taraborrelli, D., Tang, M.J., Bozem, H., Hosaynali-Beygi, Z., Axinte, R., Oswald, R., Novelli, A., Kubistin, D., Hens, K., Javed, U., Trawny, K., Breitenberger, C., Hidalgo, P.J., Ebben, C.J., Geiger, F.M., Corrigan, A.L., Russell, L.M., Ouwersloot, H.G., Vilà-Guerau de Arellano, J., Ganzeveld, L., Vogel, A., Beck, M., Bayerle, A., Kampf, C.J., Bertelmann, M., Köllner, F., Hoffmann, T., Valverde, J., González, D., Riekkola, M.-L., Kulmala, M., Lelieveld, J., 2011. The summertime Boreal forest field measurement intensive (HUMPPA-COPEC-2010): an overview of meteorological and chemical influences. Atmospheric Chemistry and Physics 11, 10599–10618. https://doi.org/10.5194/acp-11-10599-2011

Wonaschuetz, A., Sorooshian, A., Ervens, B., Chuang, P.Y., Feingold, G., Murphy, S.M., de Gouw, J., Warneke, C., Jonsson, H.H., 2012. Aerosol and gas re-distribution by shallow cumulus clouds: An investigation using airborne measurements. Journal of Geophysical Research: Atmospheres 117. https://doi.org/10.1029/2012JD018089

Wu, Z.J., Zheng, J., Shang, D.J., Du, Z.F., Wu, Y.S., Zeng, L.M., Wiedensohler, A., Hu, M., 2016. Particle hygroscopicity and its link to chemical composition in the urban atmosphere of Beijing, China, during summertime. Atmospheric Chemistry and Physics 16, 1123–1138. https://doi.org/10.5194/acp-16-1123-2016

Ye, J., Gordon, C.A., Chan, A.W.H., 2016. Enhancement in Secondary Organic Aerosol Formation in the Presence of Preexisting Organic Particle. Environ. Sci. Technol. 50, 3572–3579. https://doi.org/10.1021/acs.est.5b05512

https://doi.org/10.5194/egusphere-2025-1602
Preprint. Discussion started: 8 May 2025

Yttri, K.E., Simpson, D., Nøjgaard, J.K., Kristensen, K., Genberg, J., Stenström, K., Swietlicki, E., Hillamo, R., Aurela, M., Bauer, H., Offenberg, J.H., Jaoui, M., Dye, C., Eckhardt, S., Burkhart, J.F., Stohl, A., Glasius, M., 2011. Source apportionment of the summer time carbonaceous aerosol at Nordic rural background sites. Atmospheric Chemistry and Physics 11, 13339–13357. https://doi.org/10.5194/acp-11-13339-2011

Zhang, Q., Jimenez, J.L., Canagaratna, M.R., Allan, J.D., Coe, H., Ulbrich, I., Alfarra, M.R., Takami, A., Middlebrook, A.M., Sun, Y.L., Dzepina, K., Dunlea, E., Docherty, K., DeCarlo, P.F., Salcedo, D., Onasch, T., Jayne, J.T., Miyoshi, T., Shimono, A., Hatakeyama, S., Takegawa, N., Kondo, Y., Schneider, J., Drewnick, F., Borrmann, S., Weimer, S., Demerjian, K., Williams, P., Bower, K., Bahreini, R., Cottrell, L., Griffin, R.J., Rautiainen, J., Sun, J.Y., Zhang, Y.M., Worsnop, D.R., 2007. Ubiquity and dominance of oxygenated species in organic aerosols in anthropogenically-influenced Northern Hemisphere midlatitudes. Geophysical Research Letters 34. https://doi.org/10.1029/2007GL029979

Zhang, Y., Seigneur, C., Seinfeld, J.H., Jacobson, M., Clegg, S.L., Binkowski, F.S., 2000. A comparative review of inorganic aerosol thermodynamic equilibrium modules: similarities, differences, and their likely causes. Atmospheric Environment 34, 117–137. https://doi.org/10.1016/S1352-2310(99)00236-8

Zheng, G., Kuang, C., Uin, J., Watson, T., Wang, J., 2020. Large contribution of organics to condensational growth and formation of cloud condensation nuclei (CCN) in the remote marine boundary layer. Atmospheric Chemistry and Physics 20, 12515–12525. https://doi.org/10.5194/acp-20-12515-2020

Zieger, P., Aalto, P.P., Aaltonen, V., Äijälä, M., Backman, J., Hong, J., Komppula, M., Krejci, R., Laborde, M., Lampilahti, J., de Leeuw, G., Pfüller, A., Rosati, B., Tesche, M., Tunved, P., Väänänen, R., Petäjä, T., 2015. Low hygroscopic scattering enhancement of boreal aerosol and the implications for a columnar optical closure study. Atmospheric Chemistry and Physics 15, 7247–7267. https://doi.org/10.5194/acp-15-7247-2015